

# Distortion-Aware Brushing for Interactive Cluster Analysis in Multidimensional Projections

Hyeon Jeon, Michaël Aupetit, Soohyun Lee, Hyung-Kwon Ko, Youngtaek Kim, and Jinwook Seo

**Abstract**—Brushing is an everyday interaction in 2D scatterplots, which allows users to select and filter data points within a continuous, enclosed region and conduct further analysis on the points. However, such conventional brushing cannot be directly applied to Multidimensional Projections (MDP), as they hardly escape from False and Missing Neighbors distortions that make the relative positions of the points unreliable. To alleviate this problem, we introduce *Distortion-aware brushing*, a novel brushing technique for MDP. While users perform brushing, Distortion-aware brushing resolves distortions around currently brushed points by dynamically relocating points in the projection; the points whose data are close to the brushed data in the multidimensional (MD) space go near the corresponding brushed points in the projection, and the opposites move away. Hence, users can overcome distortions and readily extract out clustered data in the MD space using the technique. We demonstrate the effectiveness and applicability of Distortion-aware brushing through usage scenarios with two datasets. Finally, by conducting user studies with 30 participants, we verified that Distortion-aware brushing significantly outperforms previous brushing techniques in precisely separating clusters in the MD space, and works robustly regardless of the types or the amount of distortions in MDP.

**Index Terms**—Multidimensional Projections, Brushing, Multidimensional data, Distortions, Dimensionality Reduction, Visual Clustering

## 1 INTRODUCTION

Since a concept of *brushing* was first introduced by Fisherkeller et al. [1], it has become a typical interaction in visual analytics. Through brushing, users can select data points within a continuous region in the 2D space via direct manipulation, such as dragging, clicking, or lassoing [2], and focus on the points by labeling or highlighting them [3], [4]. The importance of brushing in visual analytics is also confirmed by popular visualization frameworks and libraries, such as D3.js [5] and Vega [6], which support users in easily implementing and utilizing brushing and linking.

However, conventional 2D brushing can be hardly applied to Multidimensional Projections (MDP) [7], [8] to brush the original multidimensional (MD) data, as 2D patterns and structures represented by MDP cannot precisely reflect these MD data due to distortions [8], [9], [10], [11]. For example, neighboring data in the original MD space may no longer be depicted as neighboring points in the 2D space (i.e., Missing Neighbors or MN); while non-neighboring data in the MD space might become neighboring points in the 2D space (i.e., False Neighbors or FN). MN distortions can make clusters in the MD space dispersed or split in the projection, while FN distortions may collapse or merge distinct MD clusters into a single 2D cluster. Although revealing MD cluster patterns is an important task in ex-

ploratory data analysis and visual analytics using MDP [12], [13], [14], [15], [16], such distortions make it inaccurate to brush MD clusters from their 2D projection.

Various brushing techniques [12], [17], [18], [19] specifically designed for MDP have been proposed; however, they still have several limitations. These techniques essentially work by interactively selecting a compact 2D region (2D brush) and extending it automatically to an MD region (MD brush). The set of brushed points is reported as the union [17], [18], [19] or intersection [12] of the sets of points enclosed by 2D and MD brushes. Such a workflow makes the final MD brushing vulnerable to distortions as it depends on the 2D brush—a compact region in the unfaithful projection space. Also, such brushing techniques do not give easy-to-grasp feedback to users about the quality of the MD brush as they keep positions of 2D points the same. Therefore, even a correctly brushed MD cluster can still appear as split in several components (MN distortions), or as adjacent to non-brushed points (FN distortions). Finally, MD brushes are often bound to a particular base shape (e.g., hypersphere [18], [19], hypercube [12]), and thus cannot reliably support users analyzing real-world MD data consisting of clusters with non-trivial shapes.

We propose *Distortion-aware brushing*, a novel brushing technique designed to overcome MN and FN distortions, which allows users to accurately brush clusters in the MD space from their 2D projection despite the lossy MDP process. In contrast to the previous techniques, Distortion-aware brushing locally resolves distortions through a dynamic point relocation strategy. At first, we define MD and 2D brushes as discrete sets of brushed data and their corresponding points in the MD and 2D spaces, respectively, instead of compact regions in these spaces. Then, while users proceed with brushing, the system dynamically relocates points around the 2D brush reflecting the data distribution

- Hyeon Jeon, Soohyun Lee, Jinwook Seo are with Seoul National University, Seoul, Korea. E-mail: {hj, shlee}@hcil.snu.ac.kr, jseo@snu.ac.kr
- Michaël Aupetit is with Qatar Computing Research Institute, Hamad Bin Khalifa University, Doha, Qatar. E-mail: maupetit@hbku.edu.qa
- Hyung-kwon Ko is with Naver Webtoon Corp., Seongnam, Korea. The work was done while the author was with Seoul National University. E-mail: hkko@webtooncorp.com
- Youngtaek Kim is with Samsung Electronics, Seoul, Korea. E-mail: ytaek.kim@hcil.snu.ac.kr
- Jinwook Seo and Michaël Aupetit are corresponding authors.

in the vicinity of the MD brush. Points representing data close to or far from the MD brush move near to or far from the 2D brush, respectively; therefore users can brush MD clusters more accurately. Moreover, relocation makes the 2D brush always represent MD clusters as 2D density-based clusters, such that user-generated visual clusters always match actual MD clusters. Distortion-aware brushing thus properly supports users conducting further analysis on MD data, such as detailed analysis of brushed points through linked visualizations [20], [21], or the examination of cluster structures [13], [22], [23], [24].

Meanwhile, the relocation strategy changes the original MDP layout, potentially disrupting the associated mental map, so we propose an additional interaction to transiently recover the original mapping linked to the current brush. Moreover, we add an MD similarity heatmap to verify the cluster structure formed by Distortion-aware brushing.

We demonstrate the usefulness of Distortion-aware brushing through two qualitative usage scenarios that show how the technique supports users in identifying and brushing clusters in the MD space. Moreover, we evaluate the effectiveness of Distortion-aware brushing in terms of accuracy and robustness with two quantitative user studies with 30 participants. We found that our technique significantly outperforms previous brushing techniques [12], [17], [19] in terms of accuracy, has an ability to brush non-trivial shaped clusters, and is robust to a various amount of distortions of both MN and FN types. Finally, qualitative feedback gives further insights into its usability and limitations.

## 2 BACKGROUND AND RELATED WORKS

### 2.1 Distortions in Multidimensional Projections

In recent decades, many MDP algorithms (e.g., UMAP [25], t-SNE [26], Isomap [27]) were introduced to visualize and interpret MD data. MDP represents MD data as 2D points preserving at best their original similarities, providing a visual density-based summary of the data distribution and patterns [8]. However, MDP distortions [8], [9] can interfere with important user tasks, such as analyzing clusters or detecting outliers in MD data [22], [23], [28].

MN and FN [10], [11], [29] are typical MDP distortions that affect the 2D representation of MD data patterns [8] (Figure 1). Quantitative metrics such as Trustworthiness and Continuity [30] are commonly used in practice [24], [31], [32], [33] to measure the amount of MN and FN distortions.

MDP can be enriched to visualize the amount and type of the distortions [8] by coloring points [34], [35] or a region around them using heatmaps [34], [36] or Voronoi cells [9], [10], [37]. Although these approaches are useful for interactively exploring MDP distortions and the structure of MD data, they are only visual indicators that can inform the brushing process but they do not feature brushing actions.

### 2.2 Interactive Points Relocation

Interactive point relocation is a way to overcome MDP distortions. For example, Dust-and-Magnet [38] or iPCA [39] can be used to steer the MDP layout based on the attribute values of the data. Another approach is to visualize MD data as snippet images and allow users to arrange the projection

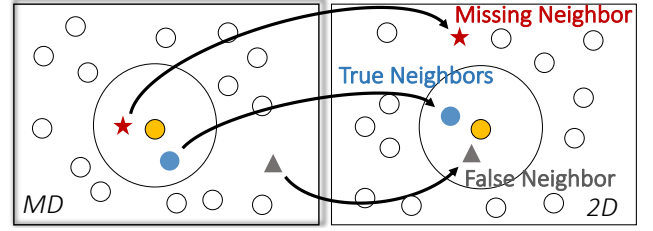


Fig. 1. True Neighbors, Missing Neighbors (MN), and False Neighbors (FN). MN and FN distortions prevent accurate brushing of MD data through their 2D projection.

to form groups by visual proximity [40]. These approaches help users explore the underlying structure of MD data and generate more reliable projections. However, they do not prevent MDP distortions and therefore cannot guarantee correct clustering of MD data with further 2D brushing.

As flawlessly preventing distortions is impossible, some previous works aimed to locally resolve errors through relocation. For example, Probing Projections [41] transiently relocates points based on their MD similarity with a user-selected point, so that it removes entire MN and FN distortions, but for the selected point only. Proxilen [42] focuses on true MD neighbors of the selected point by pushing FN to the border of a 2D magic lens centered on that point while highlighting MN with proximity coloring [9]. In contrast, instead of transiently resolving distortions around a single point, our technique performs a permanent correction of distortions related to a set of points, enabling an accurate brushing of MD clusters.

### 2.3 Brushing Multidimensional Projections

We reviewed brushing techniques for MDP in the literature and categorized them into two groups based on who determines the range of the MD brush: users manually adjust the MD brush in *axis-guided brushing* while a machine automatically constructs the MD brush based on the 2D brush in *data-guided brushing*. These techniques are summarized in Figure 2.

#### 2.3.1 Axis-Guided Brushing

The early works on brushing MDP were designed to brush along the axes. In PRIM-9 [1], brushing is done by adjusting the range of the 2D brush along two axes of an orthogonal projection forming a rectangular 2D brush. Becker et al. [3], [4] applied the same strategy to a Scatterplot Matrix (SPLOM) consisting of multiple linked orthogonal projections, showing how brushed points in one projection are clustered in the other ones. However, these techniques allow brushing on at most two axes, making difficult the discovery of MD structures that span more dimensions. To resolve this problem, Ward proposed *N*-dimensional brushing as a feature of XmdvTool [18], defining multiple 2D brushes within different projections of a SPLOM. Thus users can adjust ranges along more than two dimensions generating an MD box brush. A later version of XmdvTool [19] enables users to apply logical operators (e.g., AND, XOR) between multiple MD brushes for more flexibility.

Still, these SPLOM-based techniques have difficulty in selecting clusters lying in the MD space when clusters span

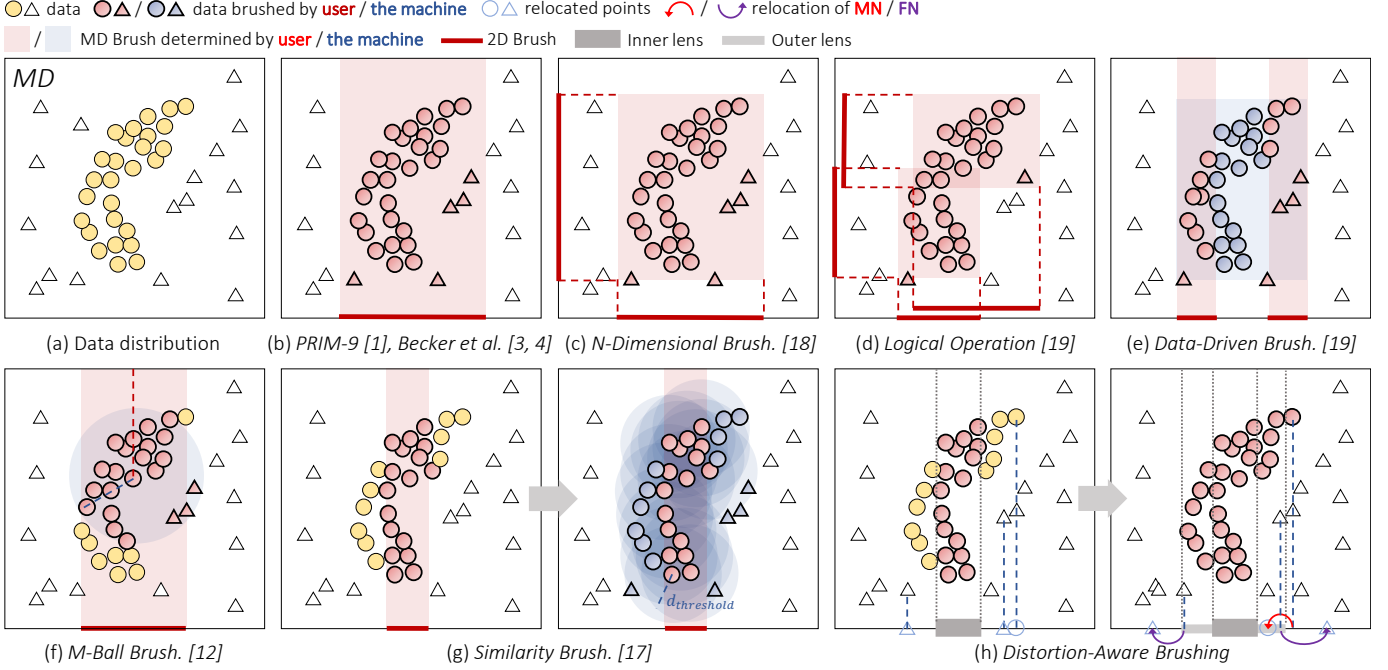


Fig. 2. State-of-the-art brushing techniques for MDP (Section 2.3.2) (a–g) and Distortion-aware brushing (h). The MD space is depicted as a 2D scatterplot in all views, and the projection is assumed to be a 1D orthogonal projection on the x-axis (b,e,f,g), or on the x and y axes (c,d). (a) We assume the user seeks to brush all MD data forming a cluster (yellow circles) except surrounding outliers (white triangles). In previous techniques (b–g), 2D brushes are represented as one or several 1D brushes (bold red lines), and MD brushes determined by users or the system are depicted as red and blue shaded areas, respectively; brushes are defined as compact regions in 2D and MD spaces, and the system reports brushed points as an intersection or a union of the points enclosed therein. In contrast, in Distortion-aware brushing (h), the technique determines 2D and MD brushes as discrete sets of points, and a 2D lens (plain grey lines) with inner (thick) and outer (thin) regions. Points are relocated in or out of the outer lens (red and purple arrows) reflecting data distribution in the vicinity of the corresponding MD brush, correcting for MN and FN distortions relative to the 2D lens (Figure 1). Users can readily brush the MD cluster through a continuous move resolving FN and MN on the fly.

more than 2 dimensions, as they impose onto visually aggregate information from multiple 2D orthogonal projections, each subject to FN distortions. Furthermore, SPLOM uses  $O(M^2)$  scatterplots for representing  $M$ -dimensional data, making brushing hardly practical when  $M$  is large. Parallel coordinate plots (PCP) [43] provide an alternative axis-based representation of MD data denser than SPLOM, for which advanced techniques for brushing have been proposed [44], [45]. However, PCP shatter the MD clusters into  $M$ -linked 1D projections (axes), each of them with an increased amount of FN distortions compared to 2D projections.

Axis-guided brushing is also not meaningful and does not generate a compact MD brush if used with nonlinear MDP techniques such as t-SNE or UMAP, because the axes of the projection space are not linear nor continuous mappings from the  $M$  original dimensions.

### 2.3.2 Data-Guided Brushing

Data-guided approaches were proposed to overcome the problems of axis-guided brushing — they follow a common workflow: (1) let users determine the 2D brush through interaction (e.g., painting); (2) automatically construct the MD brush based on the user-defined 2D brush; (3) report the brushed points as a union or intersection of the set of points within MD and 2D brushes.

For example, Data-driven brushing [19], allows users to define a 2D brush by painting certain areas in the projection, which then generates an MD brush as a minimum-size  $M$ -cube enclosing all the data corresponding to the painted points.  $M$ -ball brushing [12] works for a 2D orthogonal

projection only. Users define a circular 2D brush, which converts into an  $M$ -ball brush centered on the corresponding data in the MD space with radius determined via a statistical criterion. In both approaches, the MD brush is bounded to convex shapes, making it hard to discover non-trivial (i.e. any-shaped) clusters. In the Similarity brushing proposed by Novotný and Hauser [17], a 2D brush is a painted region, and an MD brush is defined as the data covered by the union of  $M$ -balls with radius  $\delta$  centered on the MD data corresponding to the 2D painted points. As the shape of the MD brush is determined by points covered by the 2D brush, it is not bound to convex shapes.

Still, all these MD brushes are vulnerable to MDP distortions. Indeed, the 2D brush is defined as a compact region of the projection space: if that region contains FN, the painted data might belong to more than one clusters in the MD space. Moreover, an MD cluster can be split in the projection due to MN, so the user will have to brush each of these 2D clusters separately, or even worse, will ignore them if points are spread apart not forming clear 2D clusters.

Distortion-aware brushing resolves these issues through permanent points relocation around the 2D brush: MN and FN are resolved by pulling them close to or pushing them apart from the 2D brush, respectively. In contrast to other techniques, points relocation also always generates 2D visual clusters that match with MD ones, thus giving a faithful representation matching with the user’s mental model, and allowing a better control of the interactive MD clustering process.

### 3 DESIGN OBJECTIVES

Our design objectives for Distortion-aware brushing tackle drawbacks of previous techniques (Section 2.3.2).

#### (O1) Guide brushing by visually reflecting MD clusters

Previous data-guided brushing techniques define 2D and MD brushes as compact regions in 2D and MD spaces, respectively, and deal with the MD space by converting the 2D brush into an MD brush. However, the inconceivability of the MD space makes it difficult for users to understand the conversion, thus lowering the interpretability and controllability of these techniques.

Instead, Distortion-aware brushing performs the conversion in the opposite direction: *2D points are relocated permanently to form a visual cluster that reflect an MD cluster.*

#### (O2) Allow robust brushing for any MDP distortions

Previous approaches cannot properly deal with MDP distortions as the 2D brush, a compact region of the projection space, is vulnerable to them.

By contrast, Distortion-aware brushing permanently relocates points to *ensure that 2D neighbors are always true MD neighbors and the MD cluster under focus is not split in the projection*, making the brush work robustly regardless of the type and the amount of distortions.

#### (O3) Allow accurate brushing of any-shaped MD clusters

In most previous brushing techniques [12], [18], [19], the shape of the MD brush is limited to regular compact domains, which can hardly support the discovery of clusters with non-trivial shapes typical of real-world MD data: a fixed shape can capture out-of-cluster points or miss in-cluster ones, lowering the clustering accuracy.

Distortion-aware brushing defines *MD and 2D brushes as discrete sets of points instead of compact regions*. Users can gradually append new points to the 2D brush that correspond to true MD neighbors of the already brushed points, discovering clusters with arbitrary non-trivial shapes.

## 4 DISTORTION-AWARE BRUSHING

We developed Distortion-aware brushing with a thorough investigation of our design objectives. In Section 4.1, we describe the overall workflow of the technique without technical details. Technical details are then explained along with our design choices in Section 4.2. In Section 4.3, we propose additional features, such as a transient contextual view and a heatmap of the MD similarity matrix to complement and inform the Distortion-aware brushing.

### 4.1 Workflow

The core idea of Distortion-aware brushing is to relocate points around the 2D brush by faithfully reflecting the data distribution of the MD brush and its vicinity (O1, O2). 2D and MD brushes are discrete sets of points and their corresponding data respectively (O3). The 2D brush grows progressively to form a visual cluster that reflects the MD data cluster discovered through the brushing interaction. The markers of the points in the 2D brush are painted with a unique color that identifies the brush. Brushing is done

by controlling a “painter”, which is a green disc centered on the mouse pointer whose width is controlled with the mouse wheel. The 2D brush features a magic lens [46] that operates the transient or permanent relocation process.

In a nutshell, Distortion-aware brushing consists of a 4-step workflow (Figure 3). In Step 1, the user inspects at a glance how the MD data density matches the 2D visual cluster patterns to decide the best places to initiate brushing. In Step 2, the user inspects local MN and FN distortions by hovering the painter over the points within these candidate places, color-coding each point by its MD closeness to seed points within the painter (*aff.* [9]), seeking low distortion areas. In Step 3, a short pause of the mouse move triggers a transient relocation of the points, repulsing FN and attracting MN, thus correcting the local distortions to inform the brushing decision. Moving the mouse again reverses the relocation and returns to Step 2. In Step 4, the user initiates and proceeds with brushing by dragging the painter while the mouse button is pressed, progressively capturing the covered points to form the 2D brush, while the machine iteratively performs lens construction and points relocation based on the updated 2D brush.

#### Step 1: Inspecting global density matching

The initial brush shall ideally start at a place close to the core of an actual MD cluster. Visualizing MD density can help with this task. We encode the density of the data in the MD space through the opacity of the corresponding points (Figure 3 (a); Figure 10 A-1). Through density encoding, the user can spot visual clusters (high spatial density) matching with MD clusters (high opacity) (O1, O2), and can make these locations good candidates for initiating brushing.

The density-based inspection can be done by analyzing density patterns within a single visual cluster, or by comparing 2D and MD densities between two visual clusters (Figure 4). The user can check the trustworthiness of a visual cluster by analyzing whether the within-cluster 2D density matches well with the opacity-coded MD density (Figure 4 (a-1)). In between-cluster analysis, a good candidate corresponds to a visual cluster with higher density than other visual clusters, containing points with a higher MD density than the other ones (Figure 4 ((b-1) left)). In both cases, the best location is the high-density central part of the visual cluster, which corresponds to the core region of the MD cluster. Other cases showing a density mismatch reflect MDP distortions and should be avoided (Figure 4 (a-2); (a-3); (b-1) right; (b-2)).

MD density is formally defined in Section 4.2.1.

#### Step 2: Inspecting local distortions

Step 1 gives an overview of the candidate regions, but a more stringent inspection of local distortions can help the user locate the best candidate for initiating brushing. Local MN and FN distortions can be visualized by color-coding of the MD similarity of any point to a *seed* point contained in the painter [9]. Here, as inspecting points one by one is burdensome, we extended such an approach to consider several points covered by the painter as seed points, so that users can “skim” local distortion of the projection by hovering the painter over the points. However, as seed points can become initial members of the 2D brush (when



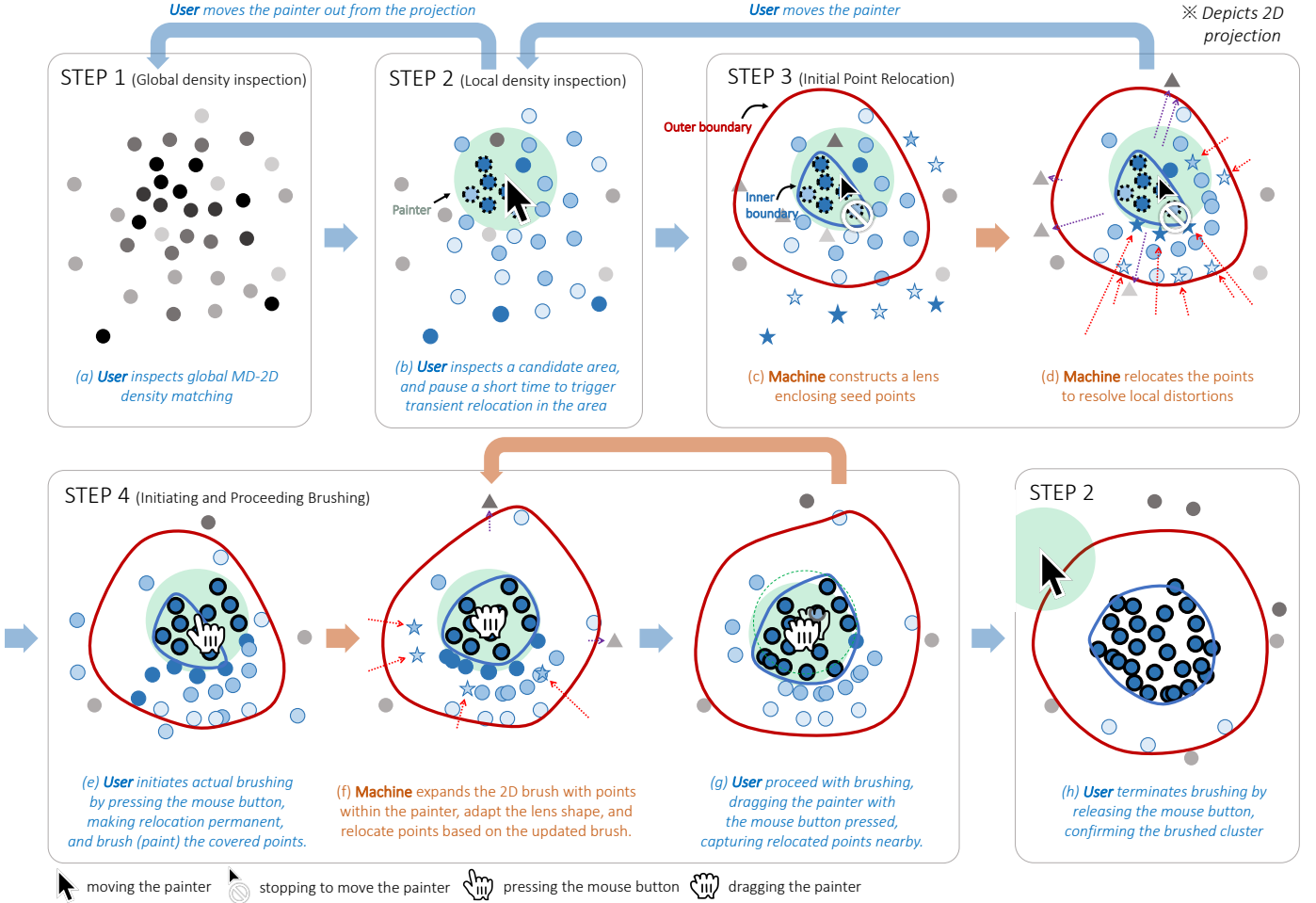


Fig. 3. Overall workflow of Distortion-aware brushing (4.1). The 2D brush features a lens with inner and outer boundaries depicted as bold blue and red closed lines, respectively. The painter is represented as a light green disc. Note that the user's actions are explained with blue text and arrow, while the machine's actions are detailed in orange. (a) The user first inspects the global reliability of a projection through the comparison of opacity-coded MD density (darker is higher) and 2D density (visual clusters) (Step 1); then (b) the user moves the painter and hovers it on points within areas with good MD and 2D density matching to explore local distortions in areas (Step 2). Distortions are visualized by coloring dots by their MD closeness (darker blue means higher closeness) to seed points in the painter (dotted edges) only for sufficiently close MD neighbors. Here, the user can go back to Step 1 by moving out the mouse from the projection. When spotting a good place to start brushing, the user pauses the painter's move for a short time. (c) The machine then constructs the lens enclosing seed points and (d) performs transient points relocation correcting for the local distortions (Step 3): FN points (triangles) move out (purple arrows), while MN points (stars) move in (red arrows). Moving the mouse again reverses the transient relocation and returns to Step 2 (b). (e) The user initiates the actual brushing by pressing the mouse button to paint the covered points (bold edges) (Step 4)—relocation then becomes permanent. (f) The machine appends the painted points to the 2D brush, updates the shape of the lens and relocates points based on the new brush. (g) The user proceeds with brushing, dragging the painter to capture relocated points nearby. By repeating (f–g), the user gradually generate a visual cluster (2D brush) which eventually faithfully represents the discovered MD cluster, (h) and terminates the brushing by releasing the mouse button; this makes the system go back to Step 2, but still means that the user stays beyond confirming the brush and is ready to start a new brush.

users press the mouse button; Step 3), not all covered points shall be seed points. Indeed, if the initial brush contains points coming from two or more distinct MD clusters, all the points further added to that brush will be true neighbors of one of these clusters with no means by which distinguish them during brushing. All new points brushed from these distinct MD clusters will erroneously agglomerate into a single visual cluster.

Therefore, we designed the system to automatically identify a set of seed points whose corresponding data form a single MD cluster. First, the system constructs a set of seed points as a subset of the covered points that forms a proper single cluster in the MD space (O2). Then, utilizing proximity coloring [9], it depicts to what extent each point in the projection has its data close to the data

corresponding to the seed points in the MD space (O1), by (1) highlighting points of close data with the current brush color (blue in Figure 3), and by (2) opacity-coding each highlighted point by the *closeness* of its data to the seed data. This graphical encoding informs the user's brushing decision (O1), identifying FN in the projection as points with bright or non-highlighted markers close to the seed points, and MN as points with dark blue markers far from the seed points.

The detailed procedure of constructing a set of seed points and the definition of *closeness* are described in Section 4.2.3 and Figure 4.2.2, respectively.

#### Step 3: Relocating points to remove distortions

Though global density (Step 1) and local distortion (Step 2) inspections support users in finding a good candidate

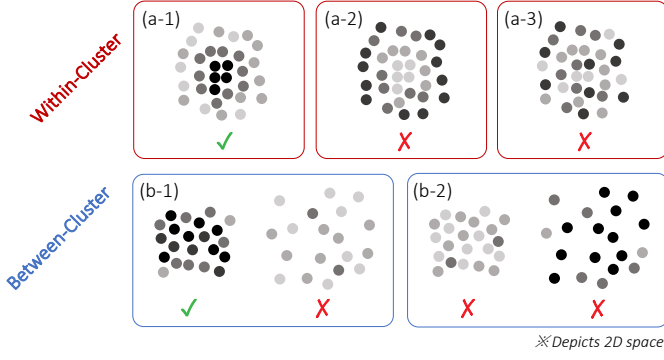


Fig. 4. Step 1: Inspecting global density matching. *Within-Cluster* analysis (top): Higher MD density (dark) is expected in the central part of a visual cluster (a-1) for a good MD-2D match, while the opposite (a-2) or random (a-3) density patterns are more likely to contain MDP distortions. *Between-Cluster* analysis (bottom): Determining low and high density regions in MD and 2D spaces is done by comparing opacity-coded MD density with 2D density of two visual clusters. (b-1) Higher MD density (dark) of points in a 2D cluster (left side) denser than another (right side), indicates a good match between MD and 2D clusters in the left one, a good place to inspect local MDP distortions. (b-2) A high density visual cluster (left) with low MD density (bright) and a low density one (right) with high MD density (dark) show a mismatch between 2D and MD clusters which are more likely to contain MDP distortions.

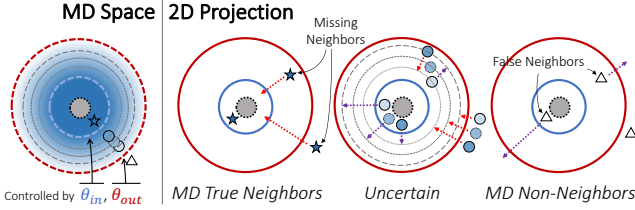


Fig. 5. Step 3: Relocating points to remove distortions. Points are relocated depending on their initial location in the projection space and the closeness of their corresponding data to the MD brush (initially, seed data). The left view sketches the data location relative to the MD brush, with one instance of *MD True Neighbors* (star), one instance of *MD Non-Neighbors* (triangle), and three instances of *Uncertain* data (circle) lying in between the other two. The bold dotted circles reflects the plain MD boundary lines of inner (blue), and outer (red) boundaries in the other views. We assume a circular 2D brush for simplicity, although it can take less regular shapes (Figure 8 (c)). The bluish color codes for the closeness of any data (Section 4.2.2) to the MD brush (the darker, the closer). The three right views show how each of these points are relocated depending on the closeness to the MD brush of their corresponding data, where the closeness is also represented as the color of point. The plain grey discs represent the area containing MD/2D brushes (initially, seed data/point). Through relocation, MN and FN distortions relative to the current brush are resolved.

region, the points nearby likely suffer from MDP distortions, not well reflecting the local MD data distribution. We thus provided a point relocation process that corrects the distortions relative to the current brush (initially, seed points within the painter itself). Following the Proxilens approach [42], users can trigger transient point relocation by halting the painter for a short time; 500 ms in our implementation (Figure 3 (b)). Correcting for local distortions can be viewed as “jumping” into the MD space, as it makes the 2D distribution around the painter and the current 2D brush better reflect the local MD data distribution. Users can reverse the current points relocation (jumping back to the 2D space) by moving the painter again.

To perform relocation, the system first constructs a magic lens around seed points in the projection, which consists of (1) a core area—the inner lens—delimited by an inner

boundary that tightly encloses seed points and (2) an annulus region around the core—the outer lens—enclosed between the inner boundary and an outer boundary (Figure 3 (c)). Afterward, points relocation is performed according to the lenses (Figure 3 (d)) so that points distribution around seed points in the projection can reflect the MD distribution around corresponding seed data (O1).

The relocation of a point depends on the closeness of its corresponding data to the seed data in the MD space (Figure 5). We partition the data into three subsets: *MD True Neighbors* are data that belong to the core MD cluster formed by the seed data (initial MD brush); *MD Non-Neighbors* denote the data that are far apart from the seed data; and *Uncertain* data are in-between the other two subsets, forming a “fuzzy” neighborhood in the MD space. Points corresponding to *MD True Neighbors* and *MD Non-Neighbors* should be part of the inner lens and external to the lens, respectively, while points corresponding to *Uncertain* data should lie within the outer lens, close to the inner boundary in proportion to their closeness to the core MD cluster. If points are already in the correct position, they stay still. Otherwise they are relocated to the correct position with an animated transition plus a remnant temporary trace for outsiders (similar to red arrows in Figure 3 (d), (f); Figure 10 B-4, E-8). Relocation corrects for the MDP distortions: points in the inner lens correspond to True Neighbors, as FN are repelled from the lens and MN are attracted within the lens.

The *Uncertain* subset and its interpolated relocation is a crucial part of Distortion-aware brushing, since it is up to users to decide whether a point will be brushed or not. The uncertain points falling into the outer lens are natural candidates for brushing; they are also geometrically the next ones that can be caught by the painter (O2). The color-coding of MD closeness informs the user’s decision (O1).

For technical details of lens construction and point relocation, refer to Section 4.2.4. The determination of the data neighbors subsets is described in Figure 4.2.2.

#### Step 4: Initiating and proceeding brushing

Once the transient relocation is settled, users can initiate brushing by pressing the mouse button (Figure 3 (e)). The system makes the relocation permanent, appends the points covered by the painter (which naturally contains seed points) and the corresponding data to 2D and MD brushes, respectively, and paints these points with the color of the brush. The system then updates the lens and relocates points based on the new brush (Figure 3 (f)). If users drag the painter while keeping the mouse button pressed (Figure 3 (g)), the brush, the painter, and the lens are updated accordingly and the relocation takes place again in a continuous cycle. Such gradual updates of the 2D brush based on the relocation enables users to update the MD brush in an arbitrary direction in the MD space, thus allowing the brushing of an MD cluster with an arbitrary shape (O3). The cycle ends when the mouse button is released, terminating brushing and confirming the brushed MD cluster (Figure 3 (h)). When the brush is terminated, the system automatically goes to Step 2, while using the union of brushed points and the points covered by the painter as seed points for local distortion visualization. Here, users can also initiate a new brushing (Section 4.3.2).

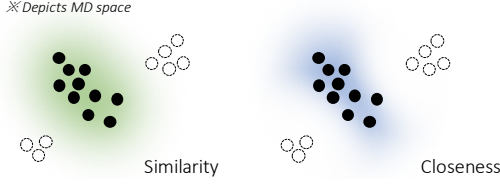


Fig. 6. Qualitative difference between similarity and closeness. The left heatmap represents how the MD similarity toward a target cluster (black dots) alters due to the position of data; high-similarity positions are depicted with more saturated color. The right heatmap represents the same for MD closeness. Unlike similarity, closeness of a datum toward a cluster is also affected by its similarity to the non-cluster points (white dots).

## 4.2 Technical Details and Design Alternatives

### 4.2.1 Defining Density (Step 1)

In Step 1, we display the MD density of each point to investigate the overall reliability of the projections. We define the MD density of a point  $p$  as  $\text{dens}(p) = \sum_{q \in P} \text{sim}(p, q)$ , borrowing the definition of Density-peak clustering [47], [48], where  $\text{sim}(p, q)$  represents the similarity between points  $p$  and  $q$ , and  $P$  denotes the entire set of points in the data.

For the similarity measure, we use the Shared-Nearest Neighbors (SNN) similarity [49] which assigns higher similarity to the pairs of points sharing more  $k$ -Nearest Neighbors ( $k$ NN). Formally, the SNN similarity between  $p$  and  $q$  is defined as  $\text{sim}(p, q) = \sum_{(m, n) \in S_{p, q}} (k+1-m) \cdot (k+1-n)$ ;  $S_{p, q}$  represents a set containing pairs  $(m, n)$  fulfilling  $p_m = q_n$  where  $p_i$  denotes an  $i$ -th nearest neighbor of  $p$ . We selected SNN as it better represents the cluster structure of high-dimensional spaces compared to other metrics (e.g.,  $k$ NN, Euclidean distance) [24], [48], [49].

### 4.2.2 Defining Closeness (Step 2–4)

Throughout the workflow, Distortion-aware brushing visually depicts the MD closeness between a datum and a set of data (a cluster) in the MD space. For example, in Step 2, the system depicts the data closeness to the seed data with opacity. In Steps 3 and 4, it performs point relocation based on the closeness. We define the closeness as a degree of membership of a datum to a cluster, such that it is higher if the datum is highly similar to more data in the cluster than to data outside the cluster.

Formally, closeness  $\text{close}_{\theta_{in}}(p, C)$  between a data  $p$  and a cluster  $C$  is defined as follows. We first define  $C(\theta_{in}, p) = \{q \in C \mid \text{sim}(p, q) > \theta_{in}\}$ , where  $\text{sim}(p, q)$  denote the similarity between data  $p$  and  $q$ , and  $\theta_{in}$  is a cutoff hyperparameter, which is controlled with a slider. In other words,  $C(\theta_{in}, p)$  represents the subset of  $C$  consisting of the points that are sufficiently close to  $p$ . Then, the average similarity of  $p$  to  $C$  is defined as  $A(\theta_{in}, p, C) = \sum_{q \in C(\theta_{in}, p)} \text{sim}(p, q) / |C(\theta_{in}, p)|$  if  $|C(\theta_{in}, p)| > 0$ , and 0 otherwise. Finally,  $\text{close}_{\theta_{in}}(p, C)$  is defined as  $\min(A(\theta_{in}, p, C) / A(0, p, P \setminus \{p\}), 1)$ . When  $A(0, p, P \setminus \{p\}) = 0$ ,  $\text{close}_{\theta_{in}}(p, C)$  is set to 1 if  $A(\theta_{in}, p, C) > 0$ , and 0 otherwise.

In Step 2, we highlight points  $p$  whose data satisfies  $\text{close}_{\theta_{in}}(p, B) > 0$  for a set of seed data  $B$ , and encode  $\text{close}_{\theta_{in}}(p, B)$  as opacity of these points.

In Steps 3 and 4, closeness is used to determine the points' relocation process. If  $\text{close}_{\theta_{in}}(p, C) = 1$ , where  $C$

is a set of seed data (Step 3) or the data corresponding to the union of the 2D brush and points covered by the painter (Step 4),  $p$  belongs to the MD *True Neighbors*. Here, we can find that  $\theta_{in}$  impacts the boundary between MD *True Neighbors* and *Uncertain*, as a higher  $\theta_{in}$  leads to less points satisfying  $\text{close}_{\theta_{in}}(p, C) = 1$  (blue bold dotted line in Figure 5). Otherwise, if  $\text{close}_{\theta_{in}}(p, C) = 0$ ,  $p$  is part of the MD *Non-Neighbors*. Finally, if  $0 < \text{close}_{\theta_{in}}(p, C) < 1$ ,  $p$  belongs to the *Uncertain* data, so the corresponding point is located close to the inner lens boundary in proportion to the closeness value of its data to  $C$ . Note that for *Uncertain* points located outside the outer boundary, we relocate only points  $p$  with  $\text{close}_{\theta_{in}}(p, C) \geq \theta_{out}$ ;  $\theta_{out}$  thus works as a threshold that controls the boundary between *Uncertain* and MD *Non-Neighbors* (red bold dotted line in Figure 5). Users can adjust  $\theta_{out}$  using a slider. The detailed procedure of the relocation considering closeness is described in Section 4.2.4.

### 4.2.3 Determining Seed Points in the Painter (Step 2-3)

In Steps 2 and 3, finding seed points among the points within the painter is needed to compute initial closeness, points relocation, and to determine the very first points to be brushed. Constructing a set of seed data  $B$  starts by finding the centroid data  $p_{center}$  with highest density among the data  $C$  whose corresponding points are in the painter:  $p_{center} = \arg \max_{p \in C} \text{dens}(p)$ . Then,  $B$  is defined as  $C(\theta_{in}, p_{center}) \cup \{p_{center}\}$  to get seed data all sufficiently close—True Neighbors—to  $p_{center}$  consistent with the definition of closeness. It avoids that False Neighbors appearing among the seed points.

### 4.2.4 Constructing the Lenses and Relocating Points (Step 3-4)

For the lens construction and points relocation procedure, we considered several design alternatives for designing the shape of the inner and outer boundaries.

**Design choice for the inner boundary (Figure 7)** We considered three alternative shapes for enclosing the brushed points: *Boundary circle*, *Convex hull*, and *Contour*. We limited the options to convex shapes, following the convention of lens boundary design [50], [51].

Beyond convexity, we wish to optimize the tightness of the inner boundary so it encloses the points limiting empty areas, making it appear as a compact homogeneous region, reflecting the fact that neighboring pairs of points within the inner lens correspond to MD True Neighbors. The purpose is for the inner lens not to precisely reflect the local MD density, but rather to reflect the connectedness of the MD data as determined by the closeness measure. A non-tight inner boundary could show disconnected components (grey areas in Figure 7 left and center), misleading the user to think the 2D brush would contain points whose data form separated MD clusters.

The *Boundary Circle* (Figure 7 left) is determined as the smallest circle enclosing the brushed points. It keeps the shape of the lens constant, although its radius would grow with the 2D brush. However, this approach often fails to tightly enclose data points, especially with outliers (red circles), leaving empty space (white areas) and possibly multiple perceptually disconnected components (grey areas).



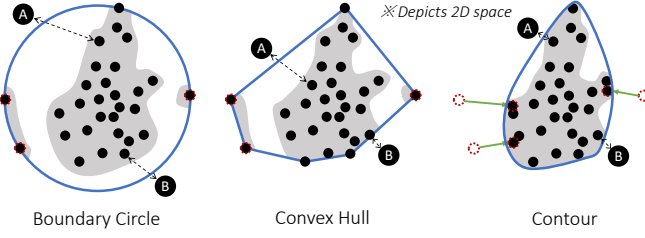


Fig. 7. Three design alternatives for the shape of the inner boundary (Section 4.2.4). We chose *Contour* as the best option as it is (1) tighter, (2) minimizes empty areas, and (3) avoids disconnectedness between components (grey areas).

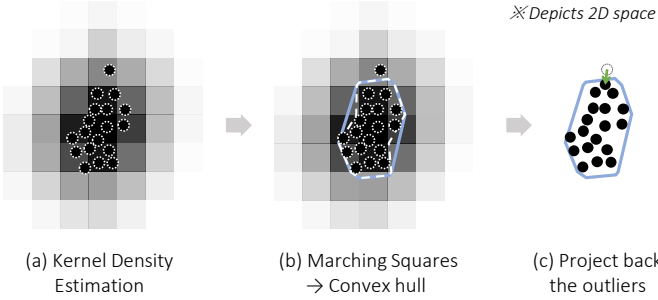


Fig. 8. The pipeline of inner lens construction. For a set of data points, (a) we first perform kernel density estimation on the grid. (b) We successively apply Marching Squares and Convex Hull algorithms to convert the grid into the inner boundary of the lens. (c) Finally, outliers are projected back to the inner boundary.

Outside points at the same distance to the inner boundary could also have a different distance to the nearest inner point (see Points A and B) impairing boundary tightness.

The *Convex Hull* (Figure 7 center) approach reduces the empty space but still suffers from multiple components (grey area) and lack of tightness (Points A and B).

The *Contour* (Figure 8 right) approach computes the convex hull of the  $\alpha$ -level contour of the 2D density of the brushed points. Outliers outside the contour are projected back to it. As a result, the inner boundary is tighter and stays as a single component, having less empty area than the contenders.

Finally, we opt for the *Contour*. In our implementation (Figure 8), we compute the 2D density using kernel density estimation [52], and compute the contour by applying Marching Squares (MSq) [53] and then Convex Hull, following an approach similar to Winglets [54]. We project outliers back to the inner lens using the interpolation procedure used for point relocation described below. The detailed procedure of inner boundary construction is given in Appendix A.

**Design choice for outer boundary and point relocation.** After designing the shape of the inner boundary enclosing  $B$ , we considered diverse ways to extend the inner boundary to construct the outer boundary and to relocate points based on the delimited outer lens. We study four design alternatives: *Scaling from the Center*, *Using Smaller MSq Threshold*, *Offsetting Edges*, and *Offsetting Corners* (Figure 9).

We considered two criteria for evaluating the quality of

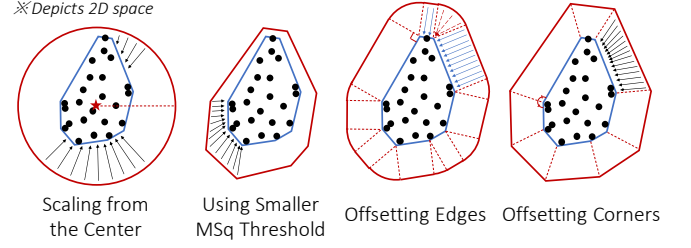


Fig. 9. Design alternatives of outer boundary construction and corresponding point relocation (Section 4.2.4). We opt for *Offsetting Corners*, considering two visual criteria: *Constancy* and *Radiality*.

a design: (1) *Constancy* of the width of the outer lens, and (2) *Radiality* of point relocation. *Constancy* is important to maintain a fixed-width margin around the inner lens free of False Neighbors, letting the user better see the uncertain points and decide about brushing them or not. The margin width should not depend on the position around the inner lens, as no direction is of specific importance in the 2D projection. *Radiality* is important to ensure that the relocation of the *Uncertain* points appears isotropic, not biased by any direction from which they originate, again because no direction is of specific importance.

The *Scaling from the Center* approach defines the outer boundary as a circle (red boundary) centered at the center of gravity of  $B$  (red star), and performs relocation (black arrows) by scaling points toward or away from that center.

The *Using smaller MSq Threshold* approach constructs the outer boundary by using the same Contour procedure as the inner boundary, but with a lower  $\alpha$  threshold for the MSq Algorithm. The relocation would follow the gradient of the density computed by the KDE.

The *Offsetting Edges* approach constructs the outer boundary by offsetting each inner boundary’s edge and connecting them with a circular arc centered on each inner boundary’s corner. Relocation happens orthogonally to the nearest inner edge (blue arrows) or corner (red arrows).

The *Offsetting Corners* approach is similar to that of *Offsetting Edges*, but constructs the outer boundary by offsetting each inner boundary’s corner along its bisector line (red dotted lines) and connecting them in the same order. The relocation direction is interpolated from the two successive bisector directions enclosing the point.

In terms of *Constancy*, *Offsetting Edges* and *Offsetting Corners* are better than the other alternatives, though the *Offsetting Corners* margin width can vary more strongly when corners have acute angles. In terms of *Radiality*, *Scaling from the Center* is the best, followed by *Offsetting Corners* and *Using Smaller MSq Threshold*. All maintain continuity of the relocation direction, while the direction of *Offsetting Edges* is constant along edges but abruptly changes at each corner.

Finally, we opt for *Offsetting Corners* which is the only alternative not failing any of the criteria. The detailed outer boundary construction and point relocation procedures are given in Appendix B.

### 4.3 Additional Features for Practical Use

We describe additional features of Distortion-aware brushing: Transient Contextualization, Multiple Brushing, and

Similarity Heatmap. These features are developed to support Distortion-aware brushing making it a complete tool for visual analytics.

#### 4.3.1 Transient Contextualization

The points relocation strategy of Distortion-aware brushing resolves distortion around the 2D brush (O2). However, the relocation could generate more distortions in other areas of the MDP, making it hard for the user to understand the 2D brushes in the context of the original MDP. To alleviate this side effect, we provided transient contextualization; when users want to see how the brushed points are located in the original projection (i.e., want to contextualize the current brushing with respect to the original projection), they can transiently pause brushing and go back to the original projection (Figure 10 C; E-1) with an animated transition by clicking a button.

#### 4.3.2 Supporting Multiple Brushes

In previous brushing techniques, multiple brushes were often provided to analyze or compare multiple sets of points at once, widening the analytic search space [12], [17], [19]. Martin and Ward [19] even proposed exploration techniques based on logical operations over multiple brushes.

We also allow users to control multiple brushes while distinguishing them with different colors. The brush color is both used for painting brushed points and for coloring other points based on the closeness measure of their data to the current brush. Users can pause the current brushing and switch the focus to another brush by pressing a button with the same brush color. In addition, we provide an *overwriting mode* and a *dragging mode* to help users better manage and update multiple brushes.

**Overwriting Mode.** While managing multiple brushes, some points can be attracted by the current brush while they already belong to other brushes. In such a case, the user can make the current brush overwrite the existing brush of these points by pressing the Control key. The color of the painter becomes blue when the mode is activated.

If the mode is not activated, attracted points from other brushes go back to their original position when the user pauses the current brushing by releasing the mouse button.

**Dragging Mode.** When previous brushes and the current brush are close, they can disturb the user to proceed with the current brushing. We let the user freely drag apart all points of a brush at once by pressing the Alt key; the color of the painter becomes yellow when that key is pressed.

#### 4.3.3 Similarity Heatmap

Estimating the similarity between clusters [55], [56] or identifying each cluster’s density [57], are both important tasks in data analysis using MDP [24]. To more readily support these tasks, we provide a heatmap view of the MD similarity matrix (Figure 10 F-11). The view depicts the SNN similarities between every pair of data in the MD space in the form of a heatmap, where each cell represents the similarity of the pair of data coded by the column and the row of that cell. Initially, the order of rows and columns in the matrix is random. As the user starts brushing, the matrix is dynamically reordered to reflect the cluster structure

progressively discovered by the brushes as square blocks along the diagonal. Cells forming blocks are color-coded by the brush color, and opacity-coded by the pairwise data SNN similarities. Cells of yet unbrushed points are colored in shades of grey.

The matrix shows (1) the size of each brush and their internal pairwise-similarities (e.g., square patterns along the diagonal within cluster  $\mathcal{A}$  in Figure 10 F-11), and (2) the between-brush similarities in the MD space (two well-separated blocks which corresponds to cluster  $\mathcal{A}$  and  $\mathcal{B}$ ), supporting cluster verification and analysis tasks.

## 5 USAGE SCENARIO

We provide usage scenarios utilizing Distortion-aware brushing for exploring two datasets. The first scenario (Section 5.1) demonstrates the main features of Distortion-aware brushing on data with a ground-truth cluster structure, and the second scenario (Section 5.2) shows how the technique can support users conducting cluster analysis of multidimensional and geospatial real-world data. In both scenarios, we assume the hyperparameters are set to default values (Appendix F).

### 5.1 Exploring the Cluster Structure of MNIST Data (Figure 10)

This usage scenario is about data analyst Alice using Distortion-aware brushing to explore unknown multidimensional data through its projection. Alice’s goal is to discover clusters and to conduct further analysis utilizing linked visualizations. Note that to illustrate how a cluster structure of the MD space can be revealed and brushed by Distortion-aware brushing, we constructed the scenario dataset with ground truth clusters by extracting data contained in three well-separated classes (labels) from the MNIST dataset [59]. We chose the class by checking the separability using the sanity-check framework [60] with the Silhouette coefficient [61] as a separability measure. The chosen classes (digits) were 0, 1, and 4. We assume that Alice uses the first two principal components from PCA [62] to generate the projection, therefore only False Neighbors distortions are expected. The projection with color-coded ground-truth classes is shown in Figure 10 (top right). All symbols below refer to that figure.

At first, Alice inspects the global density matching (Step 1) within the projection in which each point’s MD density is represented through its opacity. She finds that there exists a 2D cluster with a high 2D density (cluster  $\mathcal{A}$ ; yellow ellipse in A-1). As the points within the cluster are encoded with high opacity (i.e., high MD density), she understands that data corresponding to points in that visual cluster, are clustered as well in the MD space. However, she also notices that the cluster is not clearly separated from its surroundings (green dashed ellipses in A-1) in the projection. To identify the structure of the cluster  $\mathcal{A}$  and its surroundings more accurately, Alice moves on to the local distortion inspection (Step 2). By placing the painter on the upper and then the lower parts of the surroundings, points with shades of blue appear on both sides of cluster  $\mathcal{A}$ , showing that the surroundings are actually close to each other in the



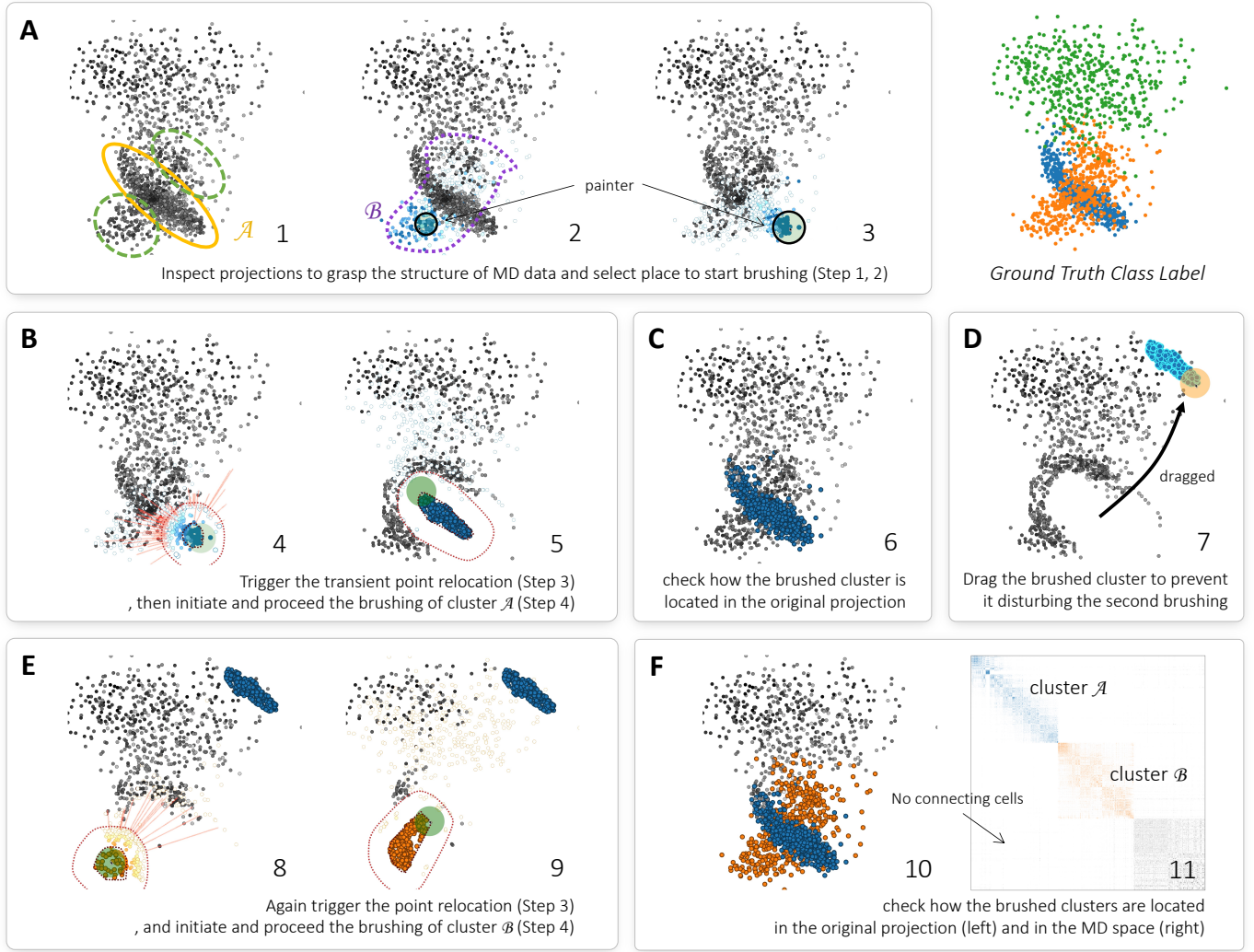


Fig. 10. Usage scenario of Distortion-aware brushing to explore the cluster structure of an unknown dataset (Section 5.1). Although two clusters overlap in the original projection (A), the user can brush each cluster individually (B, E). Note that the user can drag the firstly brushed cluster so that it cannot disturb the second brushing. The user can also check how the brushed clusters are located in the original projection (C, F-10) and analyze their mutual distance in the MD space through the similarity matrix (F-11). Note that the ground truth class label of the used data (which is MNIST) is depicted at the top right of the figure.

MD space (purple dotted contour in A-2). As a result, she hypothesizes that the surroundings actually form a single cluster in the MD space (cluster  $\mathcal{B}$ ), and are intertwined with cluster  $\mathcal{A}$  in the projection.

To check whether her hypothesis is valid, she decides to brush over the visual cluster  $\mathcal{A}$ . She first skims through that cluster and finds a place showing less local distortions at the bottom right, a good candidate place to start brushing (Step 2; A-3). By stopping there for a short time, she initiates transient points relocation (Step 3; B-4) which confirms there are few distortions there. Therefore, she starts the actual brushing (Step 4). As the brushing proceeds (B-5), the system sends members of MD cluster  $\mathcal{A}$  near the core area of the lens and pushes non-members at the edge of the lens so that Alice can visually extract the MD cluster  $\mathcal{A}$  readily. When Alice finishes brushing, she checks how data from the MD cluster  $\mathcal{A}$  were located in the original projection using Transient Contextualization (C-6).

Alice drags away cluster  $\mathcal{A}$  (D-7) to prevent visual interference with the brushing of visual cluster  $\mathcal{B}$ . She brushes visual cluster  $\mathcal{B}$  following the same process as for cluster

$\mathcal{A}$  (E-8, E-9). She then checks how points corresponding to data of MD cluster  $\mathcal{B}$  fall in the original projection using Transient Contextualization (F-10).

Now, she wants to know whether these two clusters are well-separated in the MD space, as she initially predicted. She checks the similarity heatmap view (E-11), and find that each cluster forms a well separated block of the corresponding color, along the diagonal, with few or no connecting cells out of the diagonal between these blocks, confirming her hypothesis. The heatmap also shows that the two clusters concentrate along the diagonal, each of them forming an elongated MD structure rather than a ball-shaped cluster. Moreover, the size of the blocks indicates that each of these two clusters contains about one-third of the data.

## 5.2 Exploring California Housing Dataset (Figure 11)

We will follow Bob analyzing the California housing dataset [58]. In the dataset, each data point represents an individual block that covers 1426 residents on average. A block is the smallest geographical unit used in the U.S. census. Each

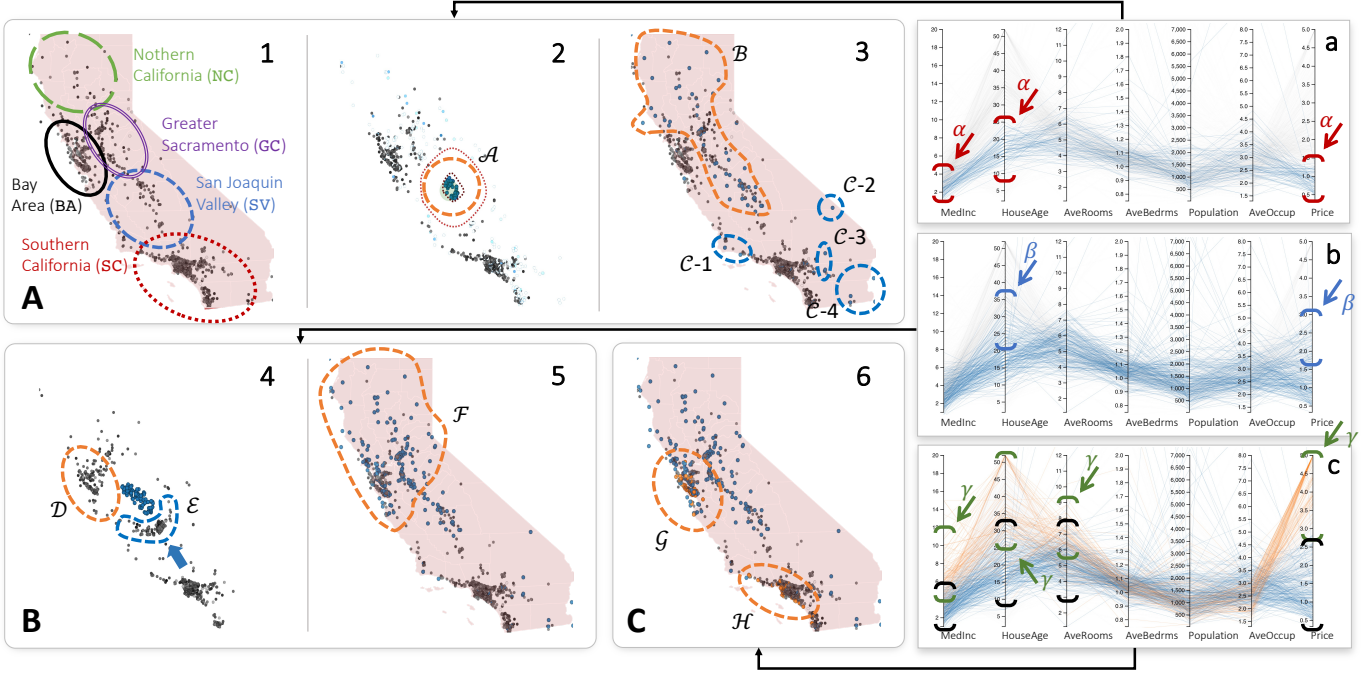


Fig. 11. Usage scenario exploring the California Housing Dataset [58] (Section 5.2). By utilizing Distortion-aware brushing and the linked parallel coordinates, the user can examine the characteristics of the clusters consisting of the blocks (i.e., the smallest geographical unit area covering 1426 individuals on average), and can understand how such clusters are distributed and located within California.

block has nine attributes, including the house prices (*Price*), the median incomes (*MedInc*), the average number of rooms (*AveRooms*), and the average age of the houses (*HouseAge*). All symbols below refer to Figure 11.

Bob’s main purpose is to find interesting clusters consisting of similar blocks and examine how and where such clusters are located and distributed within California. Bob wanted to examine clusters regarding not only the geographical proximity but also the similarity of other attributes. Therefore, in that setting, Distortion-aware brushing is applied while considering the geographical mapping of the dataset as the 2D projection, and defining the MD space as the space formed by all other attributes. The map can suffer from both FN (neighboring map location having very different attributes) and MN (map locations far apart having very similar attributes). Notice that the background map (brown area) is hidden during brushing (A-2, B-4) as the spatialization has no more direct relation to the map. Transient Contextualization can be used to display the map again (A-3, B-5, C-6).

To make further analysis about the brushed MD clusters, Bob also linked the parallel coordinates plot (PCP) [43] to the brushing. In PCP, unbrushed blocks are depicted as grey lines and brushed blocks are represented as the lines having the same color as the corresponding brush in the map.

Bob first inspects how blocks are distributed throughout California with MD density encoding (Step 1) (A-1). As a result, he identifies three 2D clusters: one in Southern California (SC; red dotted ellipse), one in the Bay Area (BA; black ellipse), and one that is elongated along Greater Sacramento (GS; purple double ellipse) and the San Joaquin Valley (SV; blue dashed ellipse). He also identified that, in the Northern California (NC; green long-dashed ellipse), there is no explicit 2D cluster, and the blocks are scattered. Note that BA and SC are in urban areas, while the others

are in rural areas.

Bob is then interested in the 2D cluster lying along SJV and GS, as it is the only cluster that lies in a rural area. He starts brushing the cluster (circle  $\mathcal{A}$  in A-2), while setting a high  $\theta_{out}$  ( $\theta_{out} = 0.95$ ) so that only the blocks that have high MD closeness to the blocks outside that area can be brushed. After brushing, Bob uses the Transient Contextualization (A-3), and finds that the MD brush contains points from SJV plus some remote blocks scattered along California, especially in rural area (SJV, GS, and NC; contour  $\mathcal{B}$  in A-3) or in the suburb of urban area (SC; ellipses  $\mathcal{C}$ -1 to  $\mathcal{C}$ -4 in A-3). Linked PCP (a) shows that the MD brush mainly contains blocks with low *MedInc*, *HouseAge*, and *Price* (red brackets with  $\alpha$ ).

Now, Bob wants to extend the search space; his goal is to identify blocks located along the rural area (SJV, GS, and NC) and having similar characteristics with the previously brushed blocks. Thus, he lowers  $\theta_{out}$  to 0.2 and resumes current brushing to “attract” points from the rural area (blue dots in B-4). While continuing brushing, he deliberately disregards blocks in SC by not brushing points relocated from the lower position to the lens (contour  $\mathcal{E}$ ; overall relocation direction is represented as blue arrow), as his main interest was the rural area.

After brushing, transient contextualization shows him that newly brushed blocks are distributed along the rural areas and BA (contour  $\mathcal{F}$  in B-5). He also identified on PCP (b) that newly brushed blocks have slightly higher *Price* and *HouseAge* (blue brackets with  $\beta$ ) compared to the previously brushed blocks represented by (a).

At this point, Bob identified several blocks within BA-GS not yet brushed (ellipse  $\mathcal{D}$  in B-4). To further examine them, Bob initiated and proceeded brushing with a new brush (orange) on these blocks. Using contextualization (C-6), Bob observes that the new MD brush contains blocks

from two geographical clusters, one in *BA* (contour  $\mathcal{G}$ ), and one in *SC* (contour  $\mathcal{H}$ ). PCP (c) also told Bob that newly brushed blocks (orange lines) have higher *MedInc*, *HouseAge*, *AveRooms*, and *Price* (green brackets with  $\gamma$ ) compared to the previously brushed cluster (blue lines). Bob concludes that there exists concentrations of “wealthy neighborhoods” in *BA* and *SC* in which people with high income live in expensive, big, and antique houses.

Disregarding points relocated from *SC* for further brushing (B-4) shows an explicit benefit of the interactivity of Distortion-aware brushing, especially compared to automatic MD clustering techniques; the user can “combine” the context of the 2D space while exploring the MD space, and thus can earn insights correlated to both spaces.

Contextualization (C-6) shows that the new MD cluster (orange dots) found in *BA* stays together with a part of the previous brush (blue dots), while another part of it lies geographically far apart in *SC*. Hence, Distortion-aware brushing allows Bob to overcome both False Neighbors and Missing Neighbors distortions.

At last, Bob performed linear discriminant analysis (LDA) in the MD space on two brushed clusters, and found that there is a clear separation between them (Appendix K). Still, in between the wealthy area (orange points) and the previously brushed points mainly in the rural area (blue points), there is no clear segmentation neither in terms of the geographical locations nor in terms of the MD attributes (orange and blue lines overlap for each attribute in the PCP; see the overlap of green and black brackets); this means that neither a naive 2D brushing in the map, nor brushing along the PCP axes could have made these two clusters stand out—yet a clear benefit of Distortion-aware brushing in this scenario.

## 6 USER STUDIES

We conducted two controlled user studies—time and accuracy comparison and robustness analysis—to evaluate the effectiveness of Distortion-aware brushing effectiveness in terms of brushing clustered points in the MD space without error. For Comparison analysis, we wanted to (1) examine whether Distortion-aware brushing outperforms previous data-guided brushing techniques [12], [17], [19] in terms of accurately brushing data clusters in the MD space and (2) check whether our brushing technique can readily brush non-trivial shaped MD clusters (O3). For Robustness analysis, our goal was to assess the extent to which our technique can work robustly regardless of the type or the amount of MDP distortions (O2). Through the wrap-up interview, we checked whether the visual identification of MD space provided by our technique truly helped participants while conducting their trials (O1).

**Task.** To evaluate the accuracy of brushing techniques, we asked participants to perform an interactive labeling task [66], [67] to identify and label clusters known to exist in the MD space but not clearly visible in the projections. Interactive labeling was picked as it is widely used to explore MD data in visual analytics [13], [66], [67], and is described as an important use case of previous brushing techniques [12], [17].

**Measurements.** We measured labeling results and task completion time of each trial. Labeling results were converted into clustering accuracy scores with respect to the ground-truth labels, using three clustering metrics: Adjusted Mutual Information (ami) [63], Adjusted Rand score (arand) [64], and V-measure (vm) [65].

**Participants.** We recruited 30 participants through an online community of a local university. Half of them (E1P1–E1P15; 13 males, 2 females; aged 19–30 [ $24.93 \pm 3.03$ ]) participated in Comparison analysis. The other half (E2P1–E2P15; 8 males, 7 females; aged 19–35 [ $24.00 \pm 4.49$ ]) participated in Robustness analysis. All participants had undergraduate level experience in statistics or linear algebra and thus could well understand the concept of MD data and brushing techniques. We rewarded each participant with the equivalent of US \$20 for their participation.

**Procedure.** One experimenter managed the experiment for all participants, one at a time. After a participant signed the consent form, the experimenter explained the concept of MD data and why 2D projections cannot precisely depict them, and then detailed the tasks and goals of the experiment. Next, during an independent session for each brushing technique (Distortion-aware brushing, plus its competitors in Comparison experiment), the experimenter first introduced and demonstrated the technique. The participant then had five minutes for practicing and asking questions. Finally, the participant conducted all the trials of that session, while labeling results and task completion times were recorded. After the session was completed, the participant answered a semi-structured wrap-up interview (Section 6.3).

**Apparatus.** All brushing techniques were executed in a Chrome web browser running on an Apple Mac Mini 2018 (Intel 8th Core i5 CPU, Intel UHD Graphics 630, 64GB RAM). Participants used techniques through a 27-inch 2K monitor with a regular mouse and keyboard setting. The projections were located in a 20cm  $\times$  20cm box at the upper left corner of the screen. We provide the screenshot of this interface in Appendix H.

**Hyperparameter.** The values set for the parameters of brushing, projections, and data preprocessing are given in Appendix G.

### 6.1 Experiment 1: Time and Accuracy Comparison

#### 6.1.1 Study Design

We compared Distortion-aware brushing with several state-of-the-art data-guided brushing techniques in terms of task’s completion time and accuracy. It was designed as a  $4 \times 2 \times 2 = 16$  within-subject experiment with three independent variables: brushing techniques (Distortion-aware brushing, Data-Driven brushing [19], *M*-Ball brushing [12], Similarity brushing [17]), task difficulty (Easy, Hard), and data source (Synthetic, Real-world).

**Brushing techniques.** To compare Distortion-aware brushing against previous brushing techniques (Figure 2, Section 2.3.2), we carefully reproduced the techniques from their original paper. We used the same graphical encoding (e.g., size of data points, design of the painter) as our implementation of Distortion-aware brushing to avoid these confounding factors. Appendix C explains the detailed workflow of the competitors.

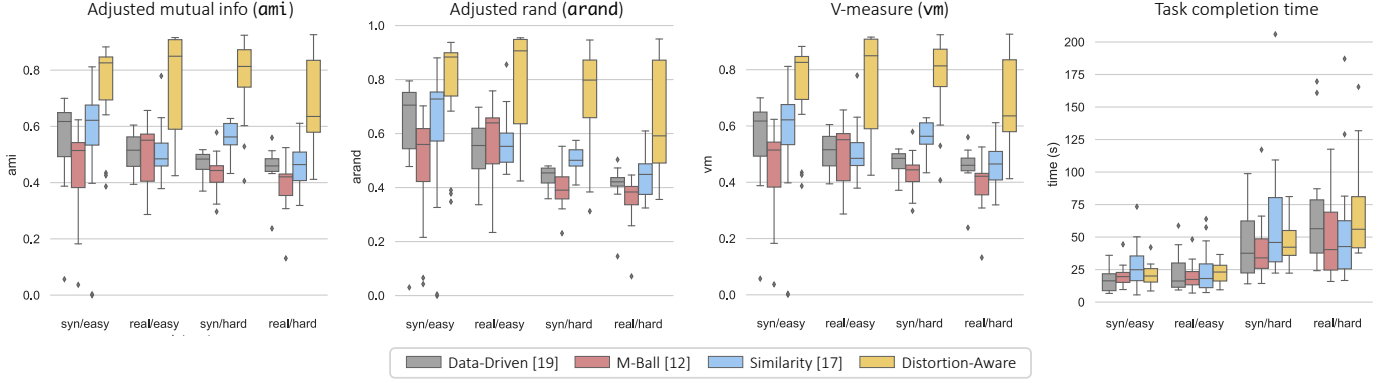


Fig. 12. Results of the time and accuracy comparisons. Three boxplots on the left depict the score of labeling tasks measured by adjusted mutual information (ami) [63], adjusted rand score (arand) [64], and v-measure [65] clustering metrics (vm), and the rightmost plot depicts task completion time. In summary, Distortion-aware brushing outperformed all the other methods in terms of accuracy while having competitive completion time.

**Task difficulties.** To add diversity to the experiment, we asked participants to complete both easy and hard tasks. For easy tasks, we used a dataset consisting of two clusters, and asked participants to extract and label a single cluster among two using each brushing technique. For hard tasks, we provided participants a dataset that consists of three clusters. Likewise, we asked them to separate and label all three clusters through multiple brushing (Section 4.3.2). We also distinguished between easy and hard tasks by using the projections with low cluster separability for hard tasks and the projections with high separability for easy tasks; we used the Silhouette coefficient [61] to measure the visual cluster separability in the 2D projections.

**Data sources.** To examine the capability of the brushing techniques to brush non-trivial clusters, we used datasets from both synthetic and real-world data sources for the experiment, which consist of hypersphere and non-trivial-shaped clusters, respectively. For the synthetic data source, we generated datasets consisting of three (for the hard task) or two (for the easy task) separated 9D hyperspheres (shells of 10D balls), each regarded as a cluster. The size of each cluster was 400 (for the hard task) and 600 (for the easy task). For the real-world data source, we constructed datasets by extracting data from three or two classes from the MNIST test dataset [59] while regarding each class as a separated cluster. We sampled half of the extracted data, which made the size of each class to be about 500. We also reduced the dimensionality of the extracted real-world datasets to 10D using PCA [62]. The reduction was performed to prevent previous brushing techniques that rely on Euclidean distances to suffer from the curse of dimensionality [68]. For both synthetic and real data sources, we checked whether the clusters are mutually separable in the MD space, utilizing the sanity-check framework [60] with the Silhouette coefficient [61] as a separability measure.

**Projections.** As Data-driven brushing [19] and *M*-ball brushing [12] can only be applied to orthogonal projections, we generated such projections for comparison. Each participant met each of the 4 pairs of data source type (synthetic/real-world) and task difficulty (easy/hard) once during each of the 4 brushing technique sessions. However, in order not to bias the results, we could not replay the same projection stimuli corresponding to a data/task pair in two

different sessions, so we needed to prepare 4 different projections (one per session) for each such pair—16 projections in total. For each pair (10D data), we generated all  ${}_{10}C_2 = 45$  possible orthogonal projections, and picked 4 projections; we made the difference between minimum and maximum ground-truth (2D) Silhouette score of these projection to be lower than 0.02 to obtain a similar visual cluster quality for all stimuli. Appendix E depicts the selected projections.

**Sessions and Trials.** All participants completed all 4 sessions of 4 trials. To minimize the order effect, we randomized the order of the sessions (brushing techniques) for each participant, and the order of the trial stimuli (data/task) within each session. There were no time limits for each trial.

### 6.1.2 Results

We used the three-way repeated measure ANOVA (RM ANOVA) [69] on task difficulties, data sources, and brushing techniques to analyze each clustering scores (ami, arand, vm). We used Bonferroni’s pairwise comparison for post hoc tests. Figure 12 depicts the result of Comparison analysis.

**Clustering accuracy score.** According to RM ANOVA, for every clustering metric, there was a significant main effect by brushing technique (ami:  $F_{3,42} = 44.518$ ,  $p < .001$ ; arand:  $F_{3,42} = 31.103$ ,  $p < .001$ ; vm:  $F_{3,42} = 44.485$ ,  $p < .001$ ). Post hoc tests validated that for all metrics, the scores of Distortion-aware brushing were significantly higher than the ones of other brushing techniques. Significant main effects were also found on task difficulty in terms of ami ( $F_{1,14} = 4.71$ ,  $p < .05$ ) and arand ( $F_{1,14} = 32.61$ ,  $p < .001$ ), but not found in terms of vm score ( $F_{1,14} = 4.58$ ,  $p = .504$ ). In addition, no interaction effects were found.

**Task completion time.** With regard to task completion time, we found main effects on task difficulties ( $F_{1,14} = 40.41$ ,  $p < .001$ ) and data sources ( $F_{1,14} = 9.32$ ,  $p < .01$ ). However, there was no significant main effect for brushing techniques ( $F_{3,42} = 1.51$ ,  $p = 0.22$ ).

We found two interaction effects: between brushing techniques and data source ( $F_{3,42} = 6.23$ ,  $p < .01$ ) and between difficulties and data sources ( $F_{1,14} = 10.22$ ,  $p < .01$ ). As our main concern is about brushing techniques, we conducted additional one-way RM ANOVA using the data source as an independent variable for each brushing techniques. We found that task completion time on real-world data is



significantly longer compared to the one on synthetic data for Distortion-aware brushing ( $F_{1,29} = 9.54, p < .01$ ), M-Ball ( $F_{1,29} = 4.47, p < .05$ ), and Data-Driven brushing ( $F_{1,29} = 7.29, p < .05$ ), but not for Similarity brushing ( $F_{1,29} = 3.89, p = .058$ ). The three-way interaction effect between all three variables was also found ( $F_{3,42} = 2.86, p < .05$ ).

### 6.1.3 Summary

Distortion-aware brushing outperformed previous techniques (Data-driven brushing, M-Ball Brushing, and Similarity Brushing) with respect to clustering accuracy, while attaining competitive completion time (Figure 12). The task completion time of brushing clusters with Distortion-aware brushing in the real-world dataset took significantly longer than brushing hyperspheres in the synthetic data. However, there was no difference in terms of task accuracy. Hence, although brushing non-trivial shaped clusters takes more time than brushing hyperspheres, Distortion-aware brushing can still do it accurately (O3).

## 6.2 Experiment 2: Robustness Analysis

### 6.2.1 Study Design

In the second experiment, we examined the robustness of Distortion-aware brushing against the amount of distortions (2A), and the type of distortions (2B). Experiment 2A was designed as a  $2 \times 6$  within-subject study consisting of two independent variables: task difficulty (easy, hard) and the amount of distortions (level 1 to 6; lower level corresponds to smaller distortions). Experiment 2B was designed identical to 2A but the amount of distortions was replaced by the type of distortions (levels 1 to 6, with 1 being the lowest level of MN and 6 being the lowest level of FN).

**Datasets** We used the fashion-MNIST test data [70] for Robustness analysis. As with the Comparison study, we extracted three (hard task) and two (easy task) classes, sampled half (i.e., about 500) of the instances from each class, and validated their separability in the MD space using the sanity-check framework [60] with the Silhouette coefficient as a separability measure. We used each class as a cluster to be discovered.

**Projections** In experiment 2A, we made six projections with decreasing reliability for each dataset (easy / hard). To pick projections that fully cover the distortions spectrum, we used the stratified sampling approach used in Pandey et al. [71] and Abbas et al. [72]. For each dataset, we first generated a 2D *t*-SNE [26] projection and normalized it in the unit square. *t*-SNE is widely used in visual analytics for visual cluster analysis [13]. Then we generated 500 noisy versions of that projection, by selecting a uniformly random proportion (range: [0-100]%) of its original points, and re-locating these points by sampling their new position from a Gaussian distribution  $X$  centered on the unit square with diagonal covariance equal to 0.166 ( $P(0 < X < 1) = 0.999$ ). Then, we evaluated each of these 500 projections using Trustworthiness & Continuity (T&C) distortion measures [30] considering 20 nearest neighbors. Trustworthiness is related to the amount of FN while Continuity focuses on MN. We represented each projection as a 2D point having the T&C measures as coordinates. We then applied

*K*-Means [73] clustering with  $K = 6$  to these 500 2D points. Finally, we picked the closest point to each of the  $K$  centroids to form the set of 6 projections covering the 2D distribution of the distortions. We sorted these 6 projections by their average T&C scores, and assigned them levels 1 to 6 following that order.

We used a similar approach for experiment 2B. Here, we utilized the NeRV [29] projection technique which allows controlling the trade-off between MN and FN by adjusting the hyperparameter  $\lambda$  from 0 to 1. Specifically, when we set  $\lambda$  close to 0, the projection tends to minimize MN but lets FN pass, while setting  $\lambda$  close to 1, it tends to minimize FN but lets MN pass.

To cover the space of MN-FN distortions, we generated 500 NeRV projections from the same dataset, with a uniform random  $\lambda$  value (range: [0-1]). We then used the same *K*-Means approach as in experiment 2A to pick the 6 NeRV projections best covering the 2D distribution of the T&C scores. We ordered the 6 projections from highest to lowest Continuity value (FN amount), and assigned them the levels 1 to 6, respectively.

Appendix D depicts the distribution of distortions made by the projections and the *K*-Means results, while the selected projections are given in Appendix E.

**Trials.** In total, each participant conducted 24 trials (12 trials for subexperiment 2A, and 12 for subexperiment 2B), all with Distortion-aware brushing. The order of the trials was randomized for each participant to avoid the order effect.

### 6.2.2 Results

We used the two-way RM ANOVA on randomization and task difficulty (for experiment 2A), or Missing-False Neighbors tradeoff and task difficulty (for experiment 2B), to analyze clustering scores and task completion time. Bonferroni's pairwise comparison was again used for post hoc tests. Figure 13 depicts the result of Robustness analysis.

**Clustering accuracy score.** In experiment 2A, RM ANOVA showed that for all metrics, there was a significant main effect by randomization (ami:  $F_{5,70} = 27.55, p < .001$ ; arand:  $F_{5,70} = 27.06, p < .001$ ; vm:  $F_{5,70} = 27.52, p < .001$ ). The post hoc test verified that the difference was made by the decrease of accuracy in levels 5 and 6, while there was no significant difference within levels 1 to 4; for all metrics, the level 5 result was significantly smaller compared to the level 1 result ( $p < .05$  for all), and the level 6 result was significantly smaller compared to the results of all other groups ( $p < .001$  for all). There was no main effect by task difficulty and no interaction effect between two independent variables for all metrics. Additional t-test showed that accuracy level reached for distortion levels 1 to 3 is consistent with the one observed for real datasets in Experiment 1 (ami:  $p = .196$ ; arand:  $p = .283$ ; vm:  $p = .197$ ).

By contrast, in experiment 2B, the analysis verified that there was no main effect by Missing-False Neighbors tradeoff (ami:  $F_{5,70} = 1.01, p = .416$ ; arand:  $F_{5,70} = 1.12, p = .356$ ; vm:  $F_{5,70} = 1.01, p = .415$ ). However, for all metrics, there existed a main effect by task difficulty (ami:  $F_{1,14} = 18.47, p < .001$ ; arand:  $F_{1,14} = 17.57, p < .001$ ; vm:  $F_{1,14} = 18.38, p < .001$ ). No interaction effect was found.



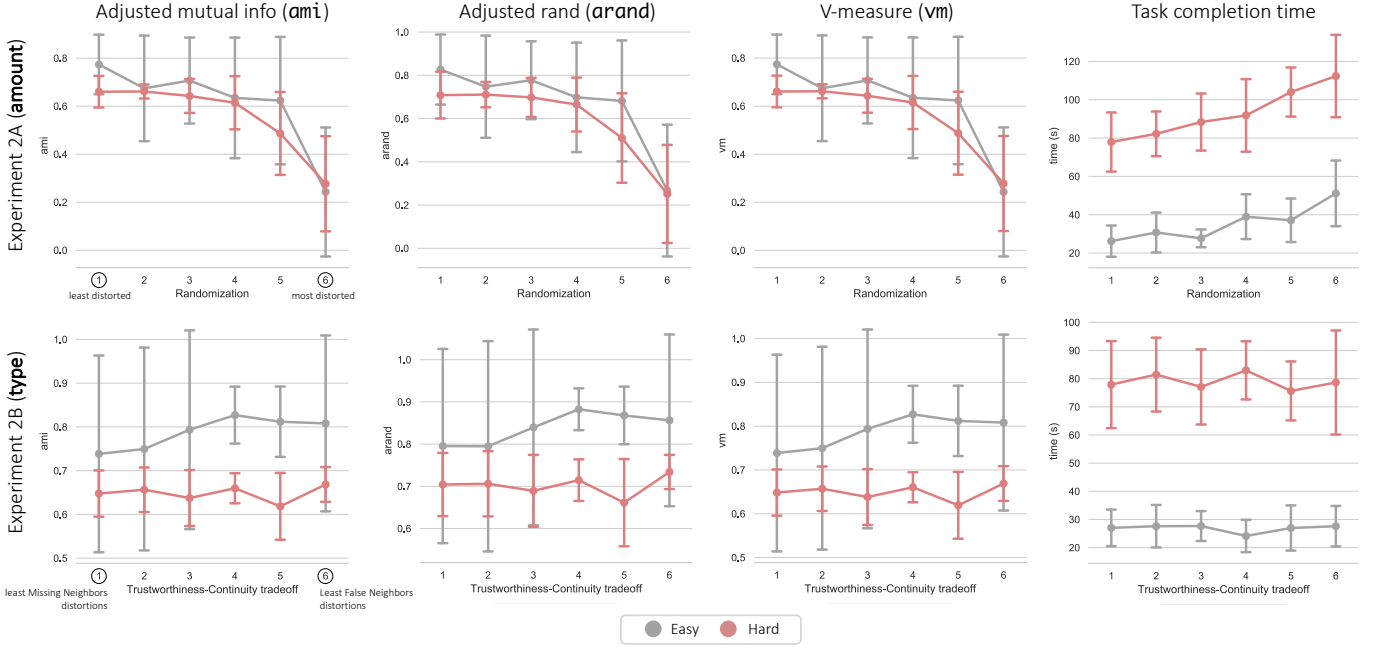


Fig. 13. Results of Robustness analysis. The first row represents the results of experiment 2A, and the second row represents the results of experiment 2B. For each row, three plots on the left depict the score of labeling tasks measured by clustering metrics and the rightmost plot depicts the task completion time, while the error bar depicts standard deviation. In experiment 2A, Distortion-aware brushing’s accuracy is robust against distortion up to level 4 for hard tasks (5 for easy ones), and then decreases abruptly. Task completion time increases steadily with the distortion level. On the other hand, experiment 2B shows that Distortion-aware brushing’s accuracy is robust to the type of distortions while easy tasks (grey) lead to more variation of the individual scores. Accuracy scores of level 1 to 3 projections are consistent with results from Experiment 1 (Figure 12) on real datasets. Time completion is not affected by the type of distortions.

**Task completion time.** In experiment 2A, we found a significant main effect by randomization ( $F_{5,70} = 25.24$ ,  $p < .001$ ). Post hoc analysis was then conducted, and verified that there was significant difference only between level 1 and level 6. Main effect by task difficulty also existed ( $F_{1,14} = 549.35$ ,  $p < .001$ ). No interaction effect was found.

In experiment 2B, there was no main effect by the tradeoff ( $F_{5,70} = .39$ ,  $p = .854$ ). We found main effect by task difficulty ( $F_{1,14} = 538.34$ ,  $p < .001$ ), and found no interaction effect.

### 6.2.3 Summary

Robustness analysis assesses that Distortion-aware brushing is robust against (1) the type of distortions, and (2) the amount of distortions until it exceeds the amount of distortions generated by level 5 projections (randomizing the position of about 80% of the data points). Such amount of distortions cannot be naturally exceeded by the projections generated by widely used MDP techniques such as *t*-SNE or PCA (Appendix I supports that claim). Thus, we can say in this experiment that Distortion-aware brushing provides accuracy scores consistent with Experiment 1, robust to an ecologically realistic amount of distortion, and to any type of them (O2).

## 6.3 Feedback from Wrap-Up Interview

In this section, we organize and report the result of the semi-structured wrap-up interviews. Our questionnaires (Appendix J) evaluated the usability, difficulty, and confidence level using Distortion-aware brushing for the participants of all the experiments, plus the other brushing techniques and how they compare to Distortion-aware brushing for the participants of Experiment 1.

### 6.3.1 Effects of Distortion-Aware Brushing features

**Global and local distortions inspection (Step 1–2).** Based on the feedback, we found that two initial steps of the Distortion-aware brushing workflow, namely inspecting global density matching (Step 1) and inspecting local distortions of a projection (Step 2), designed to help users select a proper place to start brushing, had a positive effect on users’ experience. For instance, from the Comparison experiment, 4 out of 15 (27%) participants explicitly pointed out the initial workflows as the main advantage of Distortion-aware brushing, which distinguishes it from the previous techniques. From the Robustness experiment, 13 out of 15 (87%) participants pointed out the difficulty of finding a proper place to start brushing as the factor that significantly affected the overall difficulty of brushing. E2P6 noted, “*It was convenient for me to use density encoding and distortions inspections. Some projections for which I could not find a pattern through these functionalities were hard for me to brush.*”, which indicates that participants appropriately utilized inspection functionalities to find a proper place to start brushing and felt difficulty when they could not get a hint with them.

**Points relocation (Step 3–4).** The interview results also supported the benefit of point relocation in the perspective of task accuracy. From the Comparison experiment, participants reported that it was hard for previous techniques to separate the clusters that overlap in the projection, as the projection itself stayed still and gave little hint about actual clusters in the MD space. On the other hand, many participants stated that separating clusters was much easier with Distortion-aware brushing due to points relocation. Specifically, 7 out of 15 (47%) participants reported that the points relocation strategy made brushing easier compared

to the other techniques as it allowed visual identification of MD closeness.

In addition, throughout both experiments, we found that red traces, which transiently depict the path of the points that move from outside of the lens to the inside, also helped users to more readily manage brushing. E1P1 stated, *"Through the traces, I was able to check whether I made a mistake or not, such as excessively brushing points [AN: that are not in the actual MD cluster]."*, which supports that the traces helped guide the participants not to make trivial errors. In addition, E2P9 said, *"I could confidently determine when to stop brushing through traces, by examining their decrements"*, which indicates that the participants used traces to check the current status of the brushing, as less traces mean that MN distortions related to current brushing are mostly resolved, hence the current cluster has been completed.

### 6.3.2 Benefits of Distortion-Aware Brushing in Terms of User Experience

**Improvement of user's confidence.** We found that Distortion-aware brushing helped participants to have more confidence in the brushing result and in their understanding of the MD data. E1P1 said, *"While brushing through three overlapped clusters [AN: using Distortion-aware brushing], I felt as if they are truly distinct to each other in real."*, which indicates that our technique gives the feeling of being successful at completing the task by letting the user generate visual clusters matching with actual MD clusters (O1). Similarly, E1P15 said, *"While using Distortion-aware brushing, I was able to know the real distribution of the clusters by only moving the painter across the projection."*, which means that they had confidence in their understanding of the cluster structure of the MD data with Distortion-aware brushing. By contrast, participants had less confidence about their trials while using previous brushing techniques. For example, E1P13 stated, *"[AN: While using Data-Driven Brushing], a large proportion of the decision about proceeding with brushing is given to me, and this made me somewhat cautious"*, which indicates that Data-Driven Brushing hardly gave proper feedback to enhance the user's confidence.

**Serendipity of Distortion-aware brushing.** Another unexpected benefit of Distortion-aware brushing is that users can enjoy and have fun using it. E2P5 noted, *"Using the system was like playing a game of sucking dust with a vacuum cleaner."*. In a similar context, E2P11 said, *"The red trace felt like a laser line, so it was fun for me to use the program like a game."*. Both feedback indicate that they experienced the visual feedback of points relocation as some gamification feature and had fun using the technique.

### 6.3.3 Limitations and Possible Improvements

**Disruption of the projection due to point relocation.** Although we provided contextualization of the brush within the original projection, participants mentioned that it is still hard to oversee that context during the brushing action itself. E1P5 said *"The position of an initial projection seems to be an important information, so I wonder whether it is okay to squash such information to help brushing."*, indicating that it would be better to provide information about the original projection during the brushing itself. Therefore, we plan to enhance

Distortion-aware brushing to provide initial context along with relocated points, instead of transient contextualization or space-consuming juxtaposition.

**Difficulty in terminating brushing.** Participants also reported that they had trouble in determining the boundary of the brushes. For example, E1P7 said, *"It seems that too much personal subjectivity is involved while overwriting pre-brushed points"*, which indicates that participants missed clear hints to decide when to stop brushing or to overwrite already brushed points. To resolve such problem, we could substitute point markers with more expressive MD data visualizations generating iconic small multiples [74], [75], using pictures from image data [59], or linking them to other coordinated views (Section 5.2).

## 7 DISCUSSION

### 7.1 Benefits and Limits of Points Relocation

Many MDP enrichment techniques [8] rely on a color-coding [9], [10] and few on transient point relocation [41], [42] to debunk distortions. Points relocation is the main feature of Distortion-aware brushing as it permanently corrects for the local distortions. It uses a redundant graphical encoding, adding spatialization of the MD clusters (Gestalt *grouping law of proximity* [76]) to the color encoding of MD closeness (Gestalt *grouping law of similarity*)—relocation makes *visual* the MD clusters hidden so far. Moreover, relocation engages the user in generating these visual groups, which is likely to foster trust and a feeling of empowerment [77], [78] in the clustering task, while the machine ensures brushed points are part of actual MD clusters.

However, relocation comes at the cost of losing similarity accuracy. Some small-scale FN and MN (noise) remain *within* visual clusters formed, but they are assumed not to affect the trustworthiness of the discovered cluster (signal). In contrast, maintaining accurate visual *between*-cluster similarities is largely irrelevant for the clustering task, authorizing dragging apart a 2D brush (Figure 10 D-7) to emphasize visual cluster clarity without losing accuracy.

Recent MDP [25], [26] can also emphasize cluster structures in the projection. Still, Distortion-aware brushing additionally lets the user interactively correct for distortions while it would be impossible to do so by direct manipulation of MDP hyperparameters [79], [80].

### 7.2 Scalability

Distortion-aware brushing currently handles about 5000 points (in our apparatus; Section 6). However, computations of MD closeness and the 2D brush can be distributed. Hence, the main limitations of scaling it up are the increased latency impairing fluid interaction due to lens computation, points relocation and rendering, plus visual clutter hiding color-coding of the density and MD and FN distortions. Density plots can display a sample of a large dataset without overplotting [81]. Adapting Distortion-aware brushing to density plots will be an interesting future work.

### 7.3 Limits of the studies

Orthogonal projections used in Comparison analysis cannot generate MN, so we do not know how these distortions

impact the time and accuracy of Distortion-aware brushing compared to FN. Moreover, the competing brushing techniques do not originally feature global and local inspection (Steps 1–2); both are part of Distortion-aware brushing. Hence, clustering could have been completed faster had those steps been provided. Still, it is unlikely that this absence fully explains the lower accuracy of the competitors.

## 8 CONCLUSION

Although brushing in MDP has long been considered an important research topic, previous brushing techniques for MDP exhibited difficulty in getting over distortions. To tackle this problem, we proposed Distortion-aware brushing, which essentially relocates the points to resolve the distortions and materialize MD clusters as user-generated visual groupings. Our user studies demonstrated the usefulness and usability of Distortion-aware brushing in exploring and discovering MD clusters, its robustness to distortions, and its greater accuracy compared to state-of-the-art brushing techniques. Scaling up this technique to larger datasets would be worthwhile to investigate.

## ACKNOWLEDGMENTS

This work was supported by the National Research Foundation of Korea (NRF) grant funded by the Korea government (MSIT) (No. NRF2019R1A2C208906213). The approval for the user studies was granted by Seoul National University IRB (IRB No. 2108/004-003).

## REFERENCES

- [1] M. A. Fisherkeller, J. H. Friedman, and J. W. Tukey, "Prim-9: An interactive multi-dimensional data display and analysis system," in *ACM Pacific*, 1975.
- [2] J. Heer, M. Agrawala, and W. Willett, "Generalized selection via interactive query relaxation," in *Proc. of the SIGCHI Conf. on Human Factors in Computing Systems*, ser. CHI '08. New York, NY, USA: ACM, 2008, p. 959–968.
- [3] R. A. Becker and W. S. Cleveland, "Brushing scatterplots," *Technometrics*, vol. 29, no. 2, pp. 127–142, 1987.
- [4] R. A. Becker, W. S. Cleveland, and A. R. Wilks, "Dynamic graphics for data analysis," *Statistical Science*, vol. 2, no. 4, pp. 355–383, 1987.
- [5] M. Bostock, V. Ogievetsky, and J. Heer, "D<sup>3</sup>: Data-driven documents," *IEEE Trans. on Visualization and Computer Graphics*, vol. 17, no. 12, pp. 2301–2309, 2011.
- [6] A. Satyanarayan, D. Moritz, K. Wongsuphasawat, and J. Heer, "Vega-lite: A grammar of interactive graphics," *IEEE Trans. Vis. Comput. Graphics*, vol. 23, no. 1, pp. 341–350, 2017.
- [7] E. Tejada, R. Minghim, and L. G. Nonato, "On improved projection techniques to support visual exploration of multidimensional data sets," *Information Visualization*, vol. 2, no. 4, p. 218–231, Dec. 2003.
- [8] L. G. Nonato and M. Aupetit, "Multidimensional projection for visual analytics: Linking techniques with distortions, tasks, and layout enrichment," *IEEE Trans. on Visualization and Computer Graphics*, vol. 25, no. 8, pp. 2650–2673, 2019.
- [9] M. Aupetit, "Visualizing distortions and recovering topology in continuous projection techniques," *Neurocomputing*, vol. 70, no. 7, pp. 1304–1330, 2007.
- [10] S. Lespinats and M. Aupetit, "Checkviz: Sanity check and topological clues for linear and non-linear mappings," *Computer Graphics Forum*, vol. 30, no. 1, pp. 113–125, 2011.
- [11] S. Lespinats, M. Verleysen, A. Giron, and B. Fertil, "Dd-hds: A method for visualization and exploration of high-dimensional data," *IEEE Trans. Neural Netw.*, vol. 18, no. 5, pp. 1265–1279, 2007.
- [12] M. Aupetit, N. Heulot, and J.-D. Fekete, "A multidimensional brush for scatterplot data analytics," in *IEEE Conf. on Visual Analytics Science and Technology (VAST)*, 2014, pp. 221–222.
- [13] J. Xia, Y. Zhang, J. Song, Y. Chen, Y. Wang, and S. Liu, "Revisiting dimensionality reduction techniques for visual cluster analysis: An empirical study," *IEEE Trans. Vis. Comput. Graphics*, pp. 1–1, 2021.
- [14] P. Bruneau, P. Pinheiro, B. Broeksema, and B. Otjacques, "Cluster sculptor, an interactive visual clustering system," *Neurocomputing*, vol. 150, pp. 627–644, 2015.
- [15] M. Cavallo and Demiralp, "Clustrophile 2: Guided visual clustering analysis," *IEEE Trans. on Visualization and Computer Graphics*, vol. 25, no. 1, pp. 267–276, 2019.
- [16] J. Wenskovich, I. Crandell, N. Ramakrishnan, L. House, S. Leman, and C. North, "Towards a systematic combination of dimension reduction and clustering in visual analytics," *IEEE Trans. on Visualization and Computer Graphics*, vol. 24, no. 1, pp. 131–141, 2018.
- [17] M. Novotný and H. Hauser, "Similarity brushing for exploring multidimensional relations," vol. 14, pp. 105–112, 2006.
- [18] M. Ward, "Xmdvtool: integrating multiple methods for visualizing multivariate data," in *IEEE Visualization Conf.*, 1994, pp. 326–333.
- [19] A. R. Martin and M. O. Ward, "High dimensional brushing for interactive exploration of multivariate data," in *IEEE Visualization Conf.* USA: IEEE, 1995, p. 271.
- [20] N. Pezzotti, T. Höllt, B. Lelieveldt, E. Eisemann, and A. Vilanova, "Hierarchical stochastic neighbor embedding," *Computer Graphics Forum*, vol. 35, no. 3, pp. 21–30, 2016.
- [21] W. E. Marcílio-Jr, D. M. Eler, F. V. Paulovich, J. F. Rodrigues-Jr, and A. O. Artero, "Exploretree: A focus+context exploration approach for 2d embeddings," *Big Data Research*, vol. 25, p. 100239, 2021.
- [22] R. Etemadpour, R. Motta, J. G. d. S. Paiva, R. Minghim, M. C. F. de Oliveira, and L. Linsen, "Perception-based evaluation of projection methods for multidimensional data visualization," *IEEE Trans. Vis. Comput. Graphics*, vol. 21, no. 1, pp. 81–94, 2015.
- [23] M. Brehmer, M. Sedlmair, S. Ingram, and T. Munzner, "Visualizing dimensionally-reduced data: Interviews with analysts and a characterization of task sequences," in *Proc. of the Fifth Workshop on Beyond Time and Errors: Novel Evaluation Methods for Visualization*, ser. BELIV '14. New York, NY, USA: ACM, 2014, p. 1–8.
- [24] H. Jeon, H.-K. Ko, J. Jo, Y. Kim, and J. Seo, "Measuring and explaining the inter-cluster reliability of multidimensional projections," *IEEE Trans. on Visualization and Computer Graphics*, vol. 28, no. 1, pp. 551–561, 2021.
- [25] L. McInnes, J. Healy, and J. Melville, "Umap: Uniform manifold approximation and projection for dimension reduction," 2020.
- [26] L. van der Maaten and G. Hinton, "Visualizing data using t-sne," *Journal of Machine Learning Research*, vol. 9, no. 86, pp. 2579–2605, 2008.
- [27] J. B. Tenenbaum, V. d. Silva, and J. C. Langford, "A global geometric framework for nonlinear dimensionality reduction," *Science*, vol. 290, no. 5500, pp. 2319–2323, 2000.
- [28] R. Etemadpour, L. Linsen, C. Crick, and A. Forbes, "A user-centric taxonomy for multidimensional data projection tasks," in *Proc. of the 6th Int. Conf. on Information Visualization Theory and Applications*, 2015, pp. 51–62.
- [29] J. Venna, J. Peltonen, K. Nybo, H. Aidos, and S. Kaski, "Information retrieval perspective to nonlinear dimensionality reduction for data visualization," *Journal of Machine Learning Research*, vol. 11, no. 13, pp. 451–490, 2010.
- [30] J. Venna and S. Kaski, "Local multidimensional scaling," *Neural Networks*, vol. 19, no. 6, pp. 889–899, 2006.
- [31] N. Pezzotti, J. Thijssen, A. Mordvintsev, T. Höllt, B. Van Lew, B. P. Lelieveldt, E. Eisemann, and A. Vilanova, "Gpgpu linear complexity t-sne optimization," *IEEE Trans. on Visualization and Computer Graphics*, vol. 26, no. 1, pp. 1172–1181, 2020.
- [32] L. Van Der Maaten, "Accelerating t-sne using tree-based algorithms," *J. Mach. Learn. Res.*, vol. 15, no. 1, p. 3221–3245, Jan. 2014.
- [33] C. Fu, Y. Zhang, D. Cai, and X. Ren, "Atsne: Efficient and robust visualization on gpu through hierarchical optimization," in *Proc. of the 25th ACM SIGKDD Int. Conf. on Knowledge Discovery & Data Mining*, 2019, p. 176–186.
- [34] R. M. Martins, D. B. Coimbra, R. Minghim, and A. Telea, "Visual analysis of dimensionality reduction quality for parameterized projections," *Computers & Graphics*, vol. 41, pp. 26–42, 2014.
- [35] R. M. Martins, R. Minghim, and A. Telea, "Explaining neighborhood preservation for multidimensional projections," in *Computer Graphics and Visual Computing. Eurographics-European Association for Computer Graphics*, 2015, pp. 7–14.
- [36] C. Seifert, V. Sabol, and W. Kienreich, "Stress maps: Analysing local phenomena in dimensionality reduction based visualisations," in *EuroVAST @ EuroVis*. The Eurographics Association, 2010.

- [37] N. Heulot, M. Aupetit, and J.-D. Fekete, "Proxviz: an interactive visualization technique to overcome multidimensional scaling artifacts," *Proc. of IEEE InfoVis (poster)*, vol. 2, 2012.
- [38] J. S. Yi, R. Melton, J. Stasko, and J. A. Jacko, "Dust & magnet: Multivariate information visualization using a magnet metaphor," *Information Visualization*, vol. 4, no. 4, pp. 239–256, 2005.
- [39] D. H. Jeong, C. Ziemkiewicz, B. Fisher, W. Ribarsky, and R. Chang, "ipca: An interactive system for pca-based visual analytics," *Computer Graphics Forum*, vol. 28, no. 3, pp. 767–774, 2009.
- [40] P. Joia, D. Coimbra, J. A. Cuminato, F. V. Paulovich, and L. G. Nonato, "Local affine multidimensional projection," *IEEE Trans. Vis. Comput. Graphics*, vol. 17, no. 12, pp. 2563–2571, 2011.
- [41] J. Stahnke, M. Dörk, B. Müller, and A. Thom, "Probing projections: Interaction techniques for interpreting arrangements and errors of dimensionality reductions," *IEEE Trans. on Visualization and Computer Graphics*, vol. 22, no. 1, pp. 629–638, 2016.
- [42] N. Heulot, M. Aupetit, and J. D. Fekete, "Proxilens: Interactive exploration of high-dimensional data using projections," in *EuroVis Workshop on Visual Analytics using Multidimensional Projections*. The Eurographics Association, Jun 2013.
- [43] A. Inselberg, "The plane with parallel coordinates," *The Visual Computer*, vol. 1, no. 2, pp. 69–91, 1985.
- [44] R. C. Roberts, R. S. Laramée, G. A. Smith, P. Brookes, and T. D'Cruze, "Smart brushing for parallel coordinates," *IEEE Trans. Vis. Comput. Graphics*, vol. 25, no. 3, pp. 1575–1590, 2019.
- [45] H. Hauser, F. Ledermann, and H. Doleisch, "Angular brushing of extended parallel coordinates," in *IEEE Symposium on Information Visualization*, 2002, 2002, pp. 127–130.
- [46] C. Tominski, S. Gladisch, U. Kister, R. Dachsel, and H. Schumann, "Interactive lenses for visualization: An extended survey," *Computer Graphics Forum*, vol. 36, no. 6, pp. 173–200, 2017.
- [47] A. Rodriguez and A. Laio, "Clustering by fast search and find of density peaks," *Science*, vol. 344, no. 6191, pp. 1492–1496, 2014.
- [48] R. Liu, H. Wang, and X. Yu, "Shared-nearest-neighbor-based clustering by fast search and find of density peaks," *Information Sciences*, vol. 450, pp. 200–226, 2018.
- [49] L. Ertöz, M. Steinbach, and V. Kumar, "A new shared nearest neighbor clustering algorithm and its applications," in *Workshop on Clustering High dimensional Data and its Applications at 2nd SIAM Int. Conf. on Data mining*, 2002, pp. 105–115.
- [50] C. Tominski, S. Gladisch, U. Kister, R. Dachsel, and H. Schumann, "A Survey on Interactive Lenses in Visualization," in *EuroVis - STARS*. The Eurographics Association, 2014.
- [51] M. Sarkar and M. H. Brown, "Graphical fisheye views of graphs," in *Proc. of the SIGCHI Conf. on Human Factors in Computing Systems*. New York, NY, USA: ACM, 1992, p. 83–91.
- [52] M. Rosenblatt, "Remarks on some nonparametric estimates of a density function," *The Annals of Mathematical Statistics*, vol. 27, no. 3, pp. 832 – 837, 1956.
- [53] W. E. Lorensen and H. E. Cline, "Marching cubes: A high resolution 3d surface construction algorithm," in *Proc. of the 14th Annual Conf. on Computer Graphics and Interactive Techniques*. New York, NY, USA: ACM, 1987, p. 163–169.
- [54] M. Lu, S. Wang, J. Lanir, N. Fish, Y. Yue, D. Cohen-Or, and H. Huang, "Winglets: Visualizing association with uncertainty in multi-class scatterplots," *IEEE Trans. on Visualization and Computer Graphics*, vol. 26, no. 1, pp. 770–779, 2020.
- [55] E. J. Nam, Y. Han, K. Mueller, A. Zelenyuk, and D. Imre, "Clust-sculptor: A visual analytics tool for high-dimensional data," in *2007 IEEE Symposium on Visual Analytics Science and Technology*, 2007, pp. 75–82.
- [56] J. Wenskovitch, M. Dowling, and C. North, "With respect to what? simultaneous interaction with dimension reduction and clustering projections," in *Proc. of the 25th Int. Conf. on Intelligent User Interfaces*, 2020, p. 177–188.
- [57] A. Chatzimpampas, R. M. Martins, and A. Kerren, "t-visne: Interactive assessment and interpretation of t-sne projections," *IEEE Trans. on Visualization and Computer Graphics*, vol. 26, no. 8, pp. 2696–2714, 2020.
- [58] R. Kelley Pace and R. Barry, "Sparse spatial autoregressions," *Statistics & Probability Letters*, vol. 33, no. 3, pp. 291–297, 1997.
- [59] Y. LeCun, "The mnist database of handwritten digits," <http://yann.lecun.com/exdb/mnist/>, 1998.
- [60] M. Aupetit, "Sanity check for class-coloring-based evaluation of dimension reduction techniques," in *Proc. of the Fifth Workshop on Beyond Time and Errors: Novel Evaluation Methods for Visualization*, 2014, p. 134–141.
- [61] P. J. Rousseeuw, "Silhouettes: A graphical aid to the interpretation and validation of cluster analysis," *Journal of Computational and Applied Mathematics*, vol. 20, pp. 53–65, 1987.
- [62] K. F. Pearson, "Liii. on lines and planes of closest fit to systems of points in space," *The London, Edinburgh, and Dublin Philosophical Magazine and Journal of Science*, vol. 2, no. 11, pp. 559–572, 1901.
- [63] N. X. Vinh, J. Epps, and J. Bailey, "Information theoretic measures for clusterings comparison: Variants, properties, normalization and correction for chance," *Journal of Machine Learning Research*, vol. 11, no. 95, pp. 2837–2854, 2010.
- [64] L. Hubert and P. Arabie, "Comparing partitions," *Journal of Classification*, vol. 2, pp. 193–218, 1985.
- [65] A. Rosenberg and J. Hirschberg, "V-measure: A conditional entropy-based external cluster evaluation measure," in *Proc. of the 2007 joint Conf. on empirical methods in natural language processing and computational natural language learning (EMNLP-CoNLL)*, 2007, pp. 410–420.
- [66] D. Sacha, L. Zhang, M. Sedlmair, J. A. Lee, J. Peltonen, D. Weiskopf, S. C. North, and D. A. Keim, "Visual interaction with dimensionality reduction: A structured literature analysis," *IEEE Trans. Vis. Comput. Graphics*, vol. 23, no. 1, pp. 241–250, 2017.
- [67] J. Peltonen, M. Sandholm, and S. Kaski, "Information retrieval perspective to interactive data visualization," in *Proc. of the Eurographics Conf. on Visualization (Eurovis 2013)*. The Eurographics Association, 2013, pp. 49–53.
- [68] R. Bellman, "Dynamic programming," *Science*, vol. 153, no. 3731, pp. 34–37, 1966.
- [69] R. Gueorgieva and J. H. Krystal, "Move Over ANOVA: Progress in Analyzing Repeated-Measures Data and Its Reflection in Papers Published in the Archives of General Psychiatry," *Archives of General Psychiatry*, vol. 61, no. 3, pp. 310–317, 03 2004.
- [70] H. Xiao, K. Rasul, and R. Vollgraf, "Fashion-mnist: a novel image dataset for benchmarking machine learning algorithms," 2017.
- [71] A. V. Pandey, J. Krause, C. Felix, J. Boy, and E. Bertini, "Towards understanding human similarity perception in the analysis of large sets of scatter plots," ser. CHI '16. New York, NY, USA: ACM, 2016, p. 3659–3669.
- [72] M. M. Abbas, M. Aupetit, M. Sedlmair, and H. Bensmail, "Clustme: A visual quality measure for ranking monochrome scatterplots based on cluster patterns," *Computer Graphics Forum*, vol. 38, no. 3, pp. 225–236, 2019.
- [73] J. MacQueen, "Some methods for classification and analysis of multivariate observations," in *Proc. of the fifth Berkeley symposium on mathematical statistics and probability*, vol. 1, no. 14. Oakland, CA, USA, 1967, pp. 281–297.
- [74] B. C. Kwon, H. Kim, E. Wall, J. Choo, H. Park, and A. Endert, "Axisketcher: Interactive nonlinear axis mapping of visualizations through user drawings," *IEEE Trans. on Visualization and Computer Graphics*, vol. 23, no. 1, pp. 221–230, 2017.
- [75] N. Cao, D. Gotz, J. Sun, and H. Qu, "Dicon: Interactive visual analysis of multidimensional clusters," *IEEE Trans. on Visualization and Computer Graphics*, vol. 17, no. 12, pp. 2581–2590, 2011.
- [76] S. E. Palmer, *Vision science : photons to phenomenology*. Cambridge, Mass.: MIT Press, 1999.
- [77] E. Beauxis-Aussalet, M. Behrisch, R. Borgo, D. H. Chau, C. Collins, D. Ebert, M. El-Assady, A. Endert, D. A. Keim, J. Kohlhammer, D. Oelke, J. Peltonen, M. Riveiro, T. Schreck, H. Strobel, J. J. van Wijk, and T.-M. Rhyne, "The role of interactive visualization in fostering trust in AI," *IEEE Comput Graph Appl*, vol. 41, no. 6, pp. 7–12, Nov. 2021.
- [78] T. Reis, S. Bruchhaus, B. Vu, M. X. Bornschlegl, and M. L. Hemmje, "Towards modeling AI-based user empowerment for visual big data analysis," in *CEUR Workshop co-located with CHIIR 2021, Canberra, Australia, March 19th*, I. Frommholz, H. Liu, M. Melucci, N. J. Belkin, G. J. F. Jones, N. Kando, and G. Pasi, Eds., vol. 2863, 2021, pp. 67–75.
- [79] D. Kobak and G. C. Linderman, "Initialization is critical for preserving global data structure in both t-sne and umap," *Nature Biotechnology*, vol. 39, no. 2, pp. 156–157, Feb 2021.
- [80] M. Wattenberg, F. Viégas, and I. Johnson, "How to use t-sne effectively," *Distill*, 2016. [Online]. Available: <http://distill.pub/2016/misread-tsne>
- [81] T. Trautner, F. Bolte, S. Stoppel, and S. Bruckner, "Sunspot plots: Model-based structure enhancement for dense scatter plots," *Computer Graphics Forum*, vol. 39, no. 3, pp. 551–563, 2020.